AD-A170 771 ABSORPTION AND SCATTERING BY CONDUCTIVE FIBERS: BASIC THEORY AND COMPARIS..(U) PANAMETRICS INC WALTHAM MASS N E PEDERSEN ET AL. 29 OCT 85 AFOSR-TR-86-0516 1/1

UNCLASSIFIED F49620-84-C-0045 F/G 20/3 NL

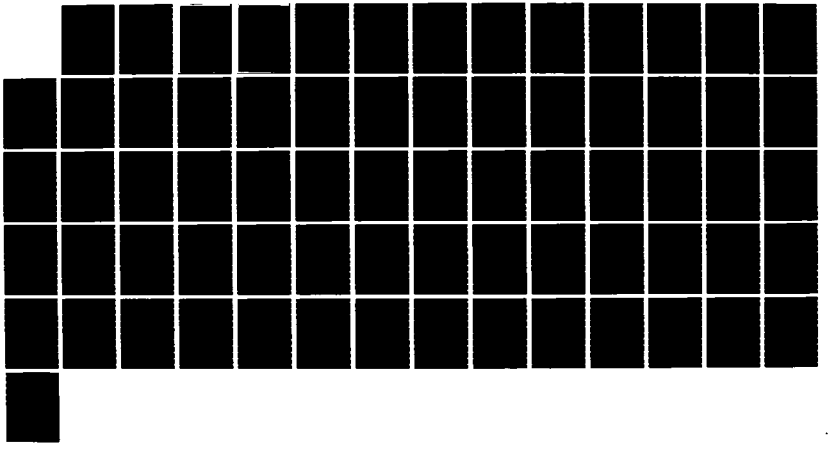

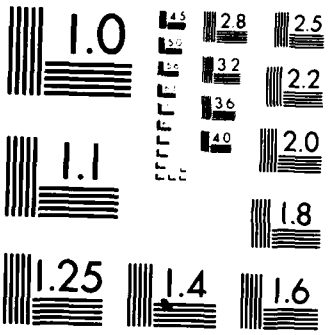

(2)

Absorption and Scattering by Conductive Fibers: Basic Theory and Comparison with Asymptotic Results

Annual Report

Contract No. F49620-84-C-0045

Prepared by

N. E. Pedersen
J. C. Pedersen
P. C. Waterman

Panametrics, Inc.
221 Crescent Street
Waltham, Massachusetts 02254

October 29, 1985

Submitted to

Major Joseph Hager
Air Force Office of Scientific Research/NE
Directorate of Electronic and Material Sciences
Spacecraft Survivability Program
Building 410
Bolling Air Force Base, DC 20332-6448

UNCLASSIFIED

SECURITY CLASSIFICATION OF THIS PAGE (When Data Entered)

REPORT DOCUMENTATION PAGE	READ INSTRUCTIONS BEFORE COMPLETING FORM
1. REPORT NUMBER AFOSR-TR- 86-0516 / 2. GOVT ACCESSION NO. AD-A170 271	3. RECIPIENT'S CATALOG NUMBER
4. TITLE (and Subtitle) Absorption and Scattering by Conductive Fibers: Basic Theory and Comparison with Asympototic Results	5. TYPE OF REPORT & PERIOD COVERED Annual Report May 1984 - Sept. 1985
	6. PERFORMING ORG. REPORT NUMBER
7. AUTHOR(s) N. E. Pedersen, J. C. Pedersen, P. C. Waterman	8. CONTRACT OR GRANT NUMBER(s) F49620-84-C-0045
9. PERFORMING ORGANIZATION NAME AND ADDRESS Panametrics, Inc. 221 Crescent Street Waltham, MA 02254	10. PROGRAM ELEMENT, PROJECT, TASK AREA & WORK UNIT NUMBERS 2306/C4
11. CONTROLLING OFFICE NAME AND ADDRESS Major Joseph Hager Air Force Office of Scientific Research/NE Directorate of Electronic & Material Sciences	12. REPORT DATE October 29, 1985
	13. NUMBER OF PAGES 64
14. MONITORING AGENCY NAME & ADDRESS(if different from Controlling Office) Spacecraft Survivability Program Building 410 Bolling Air Force Base, DC 20332-6448	15. SECURITY CLASS. (of this report) UNCLASSIFIED
	15a. DECLASSIFICATION/DOWNGRADING SCHEDULE

16. DISTRIBUTION STATEMENT (of this Report)

Approved for public release: distribution unlimited

17. DISTRIBUTION STATEMENT (of the abstract entered in Block 20, if different from Report)

18. SUPPLEMENTARY NOTES

19. KEY WORDS (Continue on reverse side if necessary and identify by block number)

Ultrathin Conductive fibers, microwave, infrared, Absorption, Electromagnetic Scattering, Obscuration

20. ABSTRACT (Continue on reverse side if necessary and identify by block number)

A theory based on the variational method, along with associated computer codes, has been developed at Panametrics for analyzing the electromagnetic scattering and absorption from thin conductive fibers of arbitrary size, conductivity and orientation. Extensions and refinements of this theory have now been completed and programmed. A summary is given of the basic equations used in the variational computation for arbitrary fibers. The quasistatic model appropriate at long wavelengths is then

DD FORM 1 JAN 73 1473 EDITION OF 1 NOV 65 IS OBSOLETE

UNCLASSIFIED

SECURITY CLASSIFICATION OF THIS PAGE (When Data Entered)

derived, followed by the infinite cylinder computation which should be accurate for wavelengths short compared with cylinder length. In order that the computations may be extended into the infrared and visible regimes, it is necessary to incorporate the optical properties of the fibers. We do this by employing the Drude Model for conductivity (or complex dielectric constant), and also introducing the dependence of conductivity on both fiber diameter and electron mean free path. Numerical results are presented for copper and lead fibers, and the approximate methods are seen to agree very well with the variational computation in those limiting regions where they should apply.

Curved fibers are considered in this report. An exact integral equation is derived for the general case, and some approximate results are then given for special fibers. Also discussed are the optimum conditions for target obscuration by a cloud of particles from a mass efficiency standpoint. Particle optimization studies are performed under varying requirements on absorption, reflection and transparency of the particle cloud.

TABLE OF CONTENTS

1.0 INTRODUCTION

During the course of the past several years, a theory based on the variational method, along with associated computer codes, has been developed at Panametrics for analyzing the electromagnetic scattering and absorption from thin conductive fibers of arbitrary size, conductivity and orientation.[1] Extensions and refinements of this theory have now been completed and programmed, as described herein.

We begin by summarizing the basic equations used in the variational computation for arbitrary fibers. The quasistatic model appropriate at long wavelengths is then derived, followed by the infinite cylinder computation which should be accurate for wavelengths short compared with cylinder length.

In order that the computations may be extended into the infrared and visible regimes, it is necessary to incorporate the optical properties of the fibers. We do this by employing the Drude model for conductivity (or complex dielectric constant), and also introducing the dependence of conductivity on both fiber diameter and electron mean free path.

Numerical results are then presented for copper and lead fibers, and the approximate methods are seen to agree very well with the variational computation in those limiting regions where they should apply.

Curved fibers are considered in Section 4. An exact integral equation is derived for the general case, and some approximate results are then given for special fibers. In Section 5, we consider the optimum conditions for target obscuration by a cloud of particles from a mass efficiency standpoint. Finally, Section 6 deals with particle optimization studies under varying requirements on absorption, reflection and transparency of the particle cloud.

2.0 THEORY

2.1 The Variational Equations

The variational method has been discussed often;[1-4] we will simply summarize the important equations here. The basic integral equation is

$$E_o \sin\theta_i e^{jkz\cos\theta_i} = I(z)\,Z + \frac{1}{2\pi}\int_0^{2\pi} \frac{j\eta k}{4\pi} \int_{-\ell/2}^{\ell/2} I(z') \left(1 + \frac{\partial^2}{k^2 \partial z'^2}\right) \times \frac{e^{-jkR}}{R}\, dz'\, d\phi' \tag{1}$$

with surface impedance Z given by

$$Z = \frac{g\, I_o(ga)}{2\pi k_o a\, (\varepsilon'' + i\varepsilon')\, I_1(ga)} \tag{2}$$

$$g^2 = k_o^2\, [(\cos^2\theta_o - \varepsilon') + i\varepsilon''] \quad .$$

For the current I(z) one assumes

$$I = I_o\, \{f_c(z) + A f_s(z)\}, \tag{3}$$

where

$$f_c(z) = \cos kz \cos qx - \cos x \cos qkz$$

$$f_s(z) = \sin kz \sin qx - \sin x \sin qkz \qquad (4)$$

$$q = \cos \theta_i \; x = k\ell/2.$$

For the constant A appearing in Eq. (3), the variational method then gives

$$A = \frac{g_s(\gamma_c - \lambda_c)}{g_c(\gamma_s - \lambda_s)}, \qquad (5)$$

in terms of the coefficients

$$\gamma_c = \frac{k}{2\pi}\int_0^{2\pi} d\phi \int_{-\ell/2}^{\ell/2}\int_{-\ell/2}^{\ell/2} f_c(z) f_c(z') \left(1 + \frac{1}{k^2}\frac{\partial 2}{\partial z'^2}\right) \frac{e^{-jkR}}{R} \, dz'dz$$

$$\gamma_s = \frac{k}{2\pi}\int_0^{2\pi} d\phi \int_{-\ell/2}^{\ell/2}\int_{-\ell/2}^{\ell/2} f_s(z) f_s(z') \left(1 + \frac{1}{k^2}\frac{\partial 2}{\partial z'^2}\right) \frac{e^{-jkR}}{R} \, dz'dz$$

$$\lambda_c = \frac{4\pi \, jZ_i}{\eta}\int_{-\ell/2}^{\ell/2} f_c^{\,2}(z)dz$$

$$\lambda_s = \frac{4\pi \, jZ_i}{\eta}\int_{-\ell/2}^{\ell/2} f_s(z)dz$$

$$g_c = k \sin \theta_i \int_{-\ell/2}^{\ell/2} f_c(z) e^{jkz \cos \theta_i} dz$$

$$g_s = k \sin \theta_i \int_{-\ell/2}^{\ell/2} f_s(z) e^{jkz \cos \theta_i} dz \qquad (6)$$

all of which can be evaluated explicitly.

The extinction, absorption and scattering cross-sections are then given explicitly by

$$\sigma_e(\theta_i) = \frac{4\pi}{k^2} \operatorname{Im}\left\{\frac{g_c^2}{\gamma_c - \lambda_c} - \frac{g_s^2}{\gamma_s - \lambda_s}\right\}$$

$$\sigma_a(\theta_i) = \frac{4\pi}{k^2} \frac{\operatorname{Re}(Z)}{|Z|} \left\{\left|\frac{g_c}{\gamma_c - \lambda_c}\right|^2 |\lambda_c| + \left|\frac{g_s}{\gamma_s - \lambda_s}\right|^2 |\lambda_s|\right\}$$

$$\sigma_s(\theta_i, \theta) = \frac{4(1-p^2)}{k^2} \left| \left(\frac{g_c}{\gamma_c - \lambda_c}\right) \left[\frac{\cos q\, x}{(1-p^2)} (\sin x \cos px - p\cos x \sin p x)\right.\right.$$

$$\left. - \frac{\cos x}{(q^2 - p^2)} (q \sin qx \cos px - p\cos qx \sin p x)\right]$$

$$+ j \left(\frac{g_s}{\gamma_s - \lambda_s}\right) \left[\frac{\sin qx}{(1-p^2)} (p \sin x \cos px - \cos x \sin px)\right.$$

$$\left.\left. - \frac{\sin x}{(q^2 - p^2)} (p \sin qx \cos px - q \cos qx \sin px)\right]\right|^2 \quad p = \cos\theta \quad x = k\ell/2 \qquad (7)$$

2.2 The Quasistatic Model

In the following, we re-derive the equations of Ref. 5 and 6 for absorption, scattering, and extinction worked out in 1965. Although the previous equations are satisfactory at radar frequencies, one must consider the relaxation effects of Sections 2.4 and 2.5 when calculating optical and infrared electromagnetic interactions.

First consider the electric field E_i inside a long, thin spheroid, given by

$$E_i = E_o - L\, 4\pi\, P, \tag{8}$$

where L = depolarizing factor, P = polarization, and E_o = homogeneous applied field. In the case of a long, thin spheroid, which is a good approximation to our conductive filament, the depolarizing factor is

$$L = 4\left(\frac{a}{\ell}\right)^2 \left[\ell n\left(\frac{\ell}{a}\right) - 1\right], \tag{9}$$

where a = particle radius and ℓ = particle length.

The definition of the polarization is

$$P = \frac{(\varepsilon - 1)\, E_i}{4\pi} \tag{10}$$

where ε = normalized dielectric constant. Combining (9) and (10) we see that the internal field is given by

$$E_i = \frac{E_o}{1 + L\,(\varepsilon - 1)} \tag{11}$$

We next take ε to be complex, i.e., $\varepsilon = \varepsilon' + i\varepsilon''$. The internal field then becomes

$$E_i = E_o \left\{ \frac{1 + L(\varepsilon' - 1)\, L\varepsilon - iL\varepsilon - iL\varepsilon''}{[L(\varepsilon' - 1) + 1]^2 + [L\varepsilon'']^2} \right\} \tag{12}$$

and we see that, in the quasistatic approximation, we have both an in-phase and a quadrature component of the internal field.

The electric dipole moment of our Rayleigh particle is defined in terms of the polarization as

$$p^{(1)} = PV_p \tag{13}$$

where V_p = particle volume. The polarizability α of the particle is related (by definition) to the dipole moment as follows:

$$p^{(1)} = \alpha E_o \ . \tag{14}$$

Combining (12), (13), and (14), we obtain the needed expression for the complex electric polarizability of the particle:

$$\alpha = \left(\frac{V_p}{4\pi}\right) \left\{\frac{(\varepsilon'-1)[1 + L(\varepsilon'-1)] + L\varepsilon''^2 + i\varepsilon''}{[L(\varepsilon'-1) + 1]^2 + [L\varepsilon'']^2}\right\} \tag{15}$$

The well known extinction theorem[6] relates the extinction cross section of any scatterer to its normalized forward scattering amplitude, S(0) by the following relation:

$$\sigma_{ext} = \frac{4\pi}{k^2} \ \text{Re}\ \{S(0)\}, \tag{16}$$

where σ_{ext} = extinction cross section, $k = 2\pi/\lambda_o$, λ_o = free space wavelength of the incident wave. Correct to order k^6, S(0) is related to the polarizability by[6]

$$S(0) = ik^3 \alpha + \frac{2}{3} k^6 \alpha^2, \tag{17}$$

where the complex polarizability is given by Eq. (15).

The absorption and scattering cross sections are, respectively, given by

$$\sigma_{abs} = 4\pi\, k\, \mathrm{Re}\,(-i\alpha) \tag{18}$$

$$\text{and} \quad \sigma_{sca} = \frac{8}{3}\,\pi k^4\,|\alpha|^2, \tag{19}$$

where α is given by Eq. (15). After considerable manipulation, the following expressions for the cross sections emerge:

$$\sigma_{ext} = kV_p\left[B + \frac{k^3 V_p}{6\pi}\,(B^2 + A^2)\right] \tag{20}$$

$$\sigma_{abs} = kV_pB \tag{21}$$

$$\sigma_{sca} = \frac{k^4 V_p^{\,2}}{6\pi}\,(A^2 + B^2) \tag{22}$$

$$A = \frac{(\varepsilon'-1) + L[(\varepsilon'-1)^2 + \varepsilon''^2]}{[1 + L(\varepsilon'-1)]^2 + [L\varepsilon'']^2} \tag{23}$$

$$B = \frac{\varepsilon''}{[1 + L(\varepsilon'-1)]^2 + [L\varepsilon'']^2} \tag{24}$$

and, in summary from the preceding sections plus Sec. 2.4 and 2.5,

$$\varepsilon' = 1 - \frac{\sigma\tau}{\varepsilon_o}\left[\frac{1}{1 + (\omega\tau)^2}\right] \tag{25}$$

$$\varepsilon'' = \frac{\sigma}{\omega\varepsilon_o}\left[\frac{1}{1 + (\omega\tau)^2}\right] \tag{26}$$

$$L = 4\left(\frac{a}{\ell}\right)^2 \left[\ell n\left(\frac{\ell}{a}\right) - 1\right] \tag{27}$$

$$\sigma = \sigma_o \left[1 - \frac{3}{8}(1-\varepsilon)\left(\frac{\Lambda}{a}\right)\right] \tag{28}$$

In an attempt to analyze the effects of Eqs. (25) and (26) on the absorption cross section, we have substituted these expressions into Eq. (24), and then inserted Eq. (24) into Eq. (21). The resulting expression for absorption cross section is too complicated for easy analysis. However, there is no doubt that in the regime of $(\omega\tau)^2 << 1$, the absorption cross section is, in general, diminished from its value without the inclusion of relaxation effects. It turns out that, for copper, $\omega\tau = 1$ corresponds to $\lambda_o \doteq 30$ microns.

We have recently shown that (at least, for the filament types of interest here), we can greatly extend the region of applicability of the quasistatic theory by letting $\ell = \pi/k_o$ in the $k_o\ell > 1$ regime. We do this only in the depolarizing factor, L', given by

$$L' = 4\left(\frac{k_o a}{\pi}\right)^2 \left[\ell n\left(\frac{\pi}{k_o a}\right) - 1\right] \tag{29}$$

Note that this substitution cannot be used to predict the scattering cross section when $k_o\ell > \pi$, and is good only for absorption. We will comment shortly on the use of this formula.

2.3 The Infinite Cylinder Approximation

Using the results of Wait[7,8] for scattering by infinitely long cylinders of arbitrary dielectric constant, we have derived the expression for absorption cross section per unit length of the infinite cylinder. The general expression, obtained by considering the inward radial component of the Poynting vector on the lateral surface of the cylinder, is

$$\sigma_a = \frac{2\pi\, a\ell \sqrt{\frac{\mu_o}{\varepsilon_o}}\, \sin^2\theta_o\, \mathrm{Re}\left[\left(\frac{ik}{\omega\mu_o}\right) J_o(k^*a) J_o'(ka)\right]}{\left| J_o(ka) - \left(\frac{1}{\mu}\right) \sin^2\theta_o \left[\ell n \left(\frac{k_o a \sin\theta_o}{2}\right) + \gamma + \frac{i\pi}{2}\right](ka) J_o'(ka) \right|^2} \quad , \tag{30}$$

$$k^2 = \mu\varepsilon\, k_o^2$$

$$\gamma = .5772$$

We have compared the results of our high frequency asymptotic quasistatic expression for the absorption cross section with this expression. The results in all (six or seven) cases were in close ($\approx$ 20%) agreement, as will be shown below. This close agreement was both surprising and gratifying to us. It is now evident that we have a quasistatic theory which can predict the <u>absorption</u> cross section of <u>thin</u> conductive filaments over a very wide range of $k\ell$, and which predicts the <u>scattering</u> cross section in the region $k_o\ell < 1$.

2.4 The Drude Model

Our early work[5,6] in the area of target obscuration was restricted to the microwave range of incident electromagnetic

energy. We did not at that time anticipate that the infrared and visible regions of the spectrum would be applicable to the absorbing particle cloud techniques which we developed. Although, during our theoretical programs with the U.S. Army Chemical Systems Lab, such applications were being explored, we were so involved in developing a comprehensive theory that we did not include the optical properties of the (metallic) filaments whose cross sections we were calculating. Indeed, it has not been until the present AFOSR program that we have included these properties. In this and the following sub-section we deal with (1) the inclusion of the optical properties in both theories, and (2) the inclusion of the dependence of electrical conductivity upon particle radius and the electron mean-free-path.

In a recent paper by Ordal, et al[9], the application of the Drude model for the prediction of complex optical dielectric constant was compared with measured values of the real and imaginary parts of the optical dielectric constant for a number of metals (Al, Cu, Au, Pb, Ag, and W). Tabular experimental results are also given for Fe, Pt, Co, Ni, Ti and Pd. This model, which is based on the free electron theory of metals, is in surprisingly good agreement with the observed experimental results. We realize, that, for certain transition elements such as Fe, the model has drawbacks. For such cases, one must resort to the use of tabular experimental data. For our present discussion, we will choose Cu as the substance comprising our fibers, and will utilize the Drude model in the calculation of the various electromagnetic cross sections. A good exposition of

this is given in Wooten's book[10], in which the normalized complex dielectric constant is derived (note that Eq. (32) corrects a mistake on p. 53 of Wooten's book):

$$\varepsilon = \varepsilon' + i\varepsilon'' \tag{31}$$

$$\varepsilon' = 1 - \frac{\omega_p^2 \tau^2}{1 + (\omega\tau)^2} \tag{32}$$

$$\varepsilon'' = \frac{\omega_p^2 \tau}{\omega[1 + (\omega\tau)^2]} \tag{33}$$

Using MKS units, the plasma frequency ω_p is given by

$$\omega_p^2 = \frac{Ne^2}{m\varepsilon_o} \tag{34}$$

in which N = electron density (m^{-3}), e = electronic change, m = effective mass of the electron, and ε_o = permittivity of free space = $(1/36\pi) \times 10^{-9}$ farads/m.

The quantity τ is the electron relaxation time, which is the time required for randomization of the momentum vector of an electron in the (metallic) lattice. For our purposes, it is instructional to cast the dielectric constant in terms of the low frequency electrical conductivity, σ, given by

$$\sigma = \frac{Ne^2\tau}{m} \tag{35}$$

From (34) and (35), we obtain

$$\omega_p^2 = \frac{\sigma}{\tau \varepsilon_o} \tag{36}$$

Using Eq. (36) in (31) and (32), we have

$$\varepsilon' = 1 - \frac{\sigma\tau}{\varepsilon_o} \left(\frac{1}{1 + (\omega\tau)^2} \right) \tag{37}$$

$$\varepsilon'' = \frac{\sigma}{\omega\varepsilon_o \left[1 + (\omega\tau)^2\right]} \quad . \tag{38}$$

Typical values of the relaxation time τ are on the order of 10^{-14} sec.

It is easily shown that Eq. (37) can be written in terms of ε'':

$$\varepsilon' = 1 - \varepsilon''(\omega\tau) \quad . \tag{39}$$

This equation shows us that, for all frequencies significantly below the visible and infrared (i.e. the microwave region), $|\varepsilon'| << |\varepsilon''|$. And, from Eq. (38), we see that ε'' goes to its low frequency value $\varepsilon'' = \sigma/\omega\varepsilon_o$ for $(\omega\tau)^2 << 1$.

The reason for the above analysis is to determine whether or not the Drude model can be utilized at <u>low</u> frequencies. Although the low frequency asymptotic value of ε' differs significantly from a value of unity, which is normally assumed for metals at <u>low</u> frequency, the ratio $|\varepsilon''/\varepsilon'|$ will always be very large when $(\omega\tau)^2$

$<< 1$. Therefore, the use of the Drude model throughout the region 10^{-6} m $\leq \lambda_o \leq 10^{-1}$ m appears to be justified, and we feel confident in using Eqs. (37) and (38) in the derivation of the electromagnetic cross sections throughout this entire wavelength range.

2.5 The Reduced Conductivity

When one or more dimensions of a conductive material (metal or semiconductor) are on the order of the mean free path of the conduction electrons, electron collisions with the surface will significantly reduce the mean free time, and hence the mean free path Λ given by

$$\Lambda = v_F \tau \tag{40}$$

where v_F = Fermi velocity and τ = relaxation time discussed previously. Since the electrical conductivity is proportional to τ (Eq. 35), the conductivity will be reduced.

The classic work on this subject was done in 1938 by Fuchs.[11] In a more recent paper, Dingle[12] reviews the subject and provides some useful numerical computations. The key equation in Dingle's paper is his Eq. (2.3) which relates the effective conductivity σ to the bulk conductivity σ_o, as a function of the mean free path Λ, the wire radius, a, and the quantity ε that is the probability of an elastic collision at the surface:

$$\sigma = \sigma_o \left[1 - \frac{3}{8} (1-\varepsilon) \left(\frac{\Lambda}{a}\right)\right] \quad . \tag{41}$$

A value of $\varepsilon = 1/2$ is frequently used as the surface scattering coefficient. Taking this, we have

$$\sigma = \sigma_o \left[1 - \frac{3}{16} \left(\frac{\Lambda}{a}\right)\right] \quad . \tag{42}$$

We have had difficulty in obtaining numerical values for mean free paths from the literature. However, Kittel[13] provides a good background as well as quantitative data for a number of metals. Taking copper as the subject material a value of $\Lambda = 4.2 \times 10^{-8}$m is given in Table 10.1 of Kittel's book. Using Eq. (40), and taking the Fermi velocity $v_F = 1.6 \times 10^6$ m/sec (Kittel, p. 240), we obtain a mean free time of $\tau = 2.6 \times 10^{-14}$ sec. This is in fairly good agreement with the value $\tau = 1.9 \times 10^{-14}$ sec, which we obtain from Ref. 9 for copper.

Utilizing the above value, we obtain for copper

$$\sigma = \sigma_o \left[1 - \frac{7.9 \times 10^{-9}}{a}\right] \tag{43}$$

where the radius a has the unit of meters. This equation shows that, if $a = 1.6 \times 10^{-8}$ m (160 Angstroms), the conductivity is roughly half its bulk value. If the radius is 0.1 micron, the conductivity is 92% of the bulk value.

This exercise was done to show that, indeed, one must consider the particle size effect upon electrical conductivity,

when computing the absorptive and extinction properties of thin metallic fibers or films.

3.0 RESULTS FOR COPPER AND LEAD FIBERS

All of the above work has been reduced to operating computer codes with quantitative graphical outputs. It should be noted that, as a part of our present AFOSR contract, we have received a Hewlett Packard HP9000 Model 520 computer. This machine will replace our present HP9835 computer, which presently requires 50 hours to complete a full set of scattering, absorption, and extinction data on a given particle over a wavelength range from 10 cm to 1 micron. The new machine will reduce this time by a factor of between 100X and 1000X.

As a first example, consider copper. We take fiber radius of 5×10^{-8} m, unreduced bulk conductivity of 5.8×10^{7} mho/m, relaxation time 1.9×10^{-14} sec, mean free path of 3×10^{-8} m. The reduced conductivity can now be computed from Eq. (42), and using that result the complex optical dielectric constant is obtained from Eqs. (37) and (38). Results of this computation are plotted in Fig. 1 vs. wavelength over the range from 10 cm to 1 micron.

Knowing ε' and ε'', the surface impedance of the fiber may be computed from Eq. (2). The results, which are again frequency-dependent, are shown in Fig. 2.

Choosing a fiber length of 5×10^{-4} m, the extinction, absorption and scattering cross-sections may now be obtained from Eq. (7) of the variational method, and are plotted vs. wavelength in Fig. 3. Note that both the scattering and absorption cross-sections rise to peak values at $\lambda \sim 10^{-3}$ m, then fall off. The extinction cross-section must equal the sum of the scattering and absorption cross-sections, and this is seen to be accurately obeyed except at the shorter wavelengths $\lambda \lesssim 10^{-4}$ m, where we believe that σ_s is in error due to employing too few points in the numerical integration (which affects only σ_s).

In Fig. 4 we show the cross-sections obtained using the quasistatic theory, for the same example. As expected, both σ_a and σ_s are in excellent agreement with the previous values at the longer wavelengths. The absorption cross-section moreover, is seen to agree with that of Fig. 3 for the shorter wavelengths also, providing good confirmation of the high frequency depolarizing factor proposed in Eq. (29).

In Fig. 5 σ_a is plotted using the infinite cylinder approximation Eq. (30) appropriate for short wavelengths. Almost exact agreement is found with both preceding results, for $\lambda \lesssim 10^{-3}$ m, and hence for $k\ell \gtrsim 3$, about as one would expect.

Figures 6 and 7 give respectively the variational and quasistatic results for the same cylinder, but shorter by a factor of ten. The peaking and crossover behavior from long to short wavelength is now seen to occur at $\lambda \sim 10^{-4}$ m as one would

anticipate. Agreement between the two figures is analogous to that of the first example, although the peak height predicted by the quasistatic theory for σ_a is seen to be somewhat low this time. For the infinite cylinder approximation, the curve of Fig. 5 applies without change, and again σ_a is in excellent agreement with the variational values at the shorter wavelengths for which $k\ell \gtrsim 3$.

Next, consider lead fibers. The resulting dielectric constant and impedance are shown vs. wavelength in Figs. 8 and 9, with fiber parameters as listed in the figures. The variational results, along with the long and short wavelength approximations, are shown in Figs. 10-12, respectively. Agreement is analogous to that obtained with copper. Note that in these cases σ_a shows saturation effects for wavelengths $\gtrsim 10^{-5}$ m.

Figures 13 and 14 show that upon increasing the fiber radius by a factor of 10, the dielectric constant is substantially unchanged, while the surface impedance decreases at all wavelengths by about two orders of magnitude. The resulting cross-sections, given in Figs. 15-17, again show the same pattern of agreement between the variational (Fig. 15) and approximate results.

Finally, Figs. 18 and 19 (which should be compared with the short wavelength approximation of Fig. 17) give the corresponding values when the fiber length is decreased by a factor of ten. This time the absorption cross-section peaks at $k\ell \sim 3$, precisely as observed originally with copper.

The agreement seen consistently throughout these computations provides striking confirmation of the validity of the variational results, and also provides some explicit bounds on the regimes in which either of the approximate methods might safely be used independently.

4.0 SCATTERING BY CURVED CONDUCTIVE FIBERS

4.1 Preliminary Survey

All the numerical results obtained by Panametrics to the present time for scattering and absorption by conductive fibers have dealt with straight fibers. The question naturally arises then as to the effects of curvature of the fibers on the scattering and absorption efficiency.

A search of the literature reveals very little work on curved wires; all of that, with two exceptions, involving perfectly conducting wires. The curved, perfectly conducting wire was apparently first considered by Aharoni in 1946.[14] His equations were applied to circular loop and spiral antennas by Mei.[15] In 1956 Kouyoumjian considered back-scattering from perfectly conducting circular loops.[16] The two exceptions to the perfectly conducting case are the work of Philipson, who considered lossless dielectric rings,[17] and Acquista, who considered wavy cylinders.[18] In both of these latter cases, however, the scatterer was taken to be only a perturbation on its surroundings, so that a full integral equation approach was not required.

We have derived the integral equation for curved fibers, having finite conductivity, from first principles. The usual thin-wire analysis invariably assumes that the electric field can be expressed in terms of a current filament concentrated on the axis of the fiber, and this is physically somewhat unsatisfactory especially when, as in the present case, we must work with both electric and magnetic fields at the surface of the fiber. We use instead an approach based on Huygen's principle,[19] which states that fields generated by the tangential components of E and H (distributed along the surface of the fiber) must precisely cancel the axial components of the incident electric field along the fiber axis.

This results in an equation involving integrals of the two unknown *functions E and H along the fiber.* Taking the thin-wire limit where fiber radius is very small compared to incident wavelength, the second of these integrals is fairly straightforward, and for good conductors is interpretable as the field due to a distribution of surface currents. The first integral behaves differently, however. The kernel reduces to a delta-function, resulting in a term in E at the field point of evaluation of the integral equation. Surface values of E and H can then be related by a surface impedance concept to finally give a pure integral equation for the current.

4.2 The Integral Equation

When an incident electromagnetic field $\underline{E}^{inc}$ illuminates a body in free space, the resulting fields are related by Huygens' principle, which states rigorously that[19]

$$\underline{E}^{inc}(\underline{r}) - (1/4\pi)\,\nabla \times \int d\sigma' \hat{kn}' \times \underline{E}_+(\underline{r}')\; g(kR)$$

$$-(1/4\pi)\,\nabla \times \nabla \times \int d\sigma' \hat{in}' \times \underline{H}_+(\underline{r}')\; g(kR) = \begin{cases} \underline{E}(\underline{r}) & \text{outside} \\ 0 & \text{inside} \end{cases} . \qquad (44)$$

The left-hand side (LHS) of this equation consists of the sum of the electric fields due to the incident wave and surface distributions over the body of magnetic and electric dipoles, respectively. Here

$$g(kR) = (1/kR)e^{ikR}, \quad R = |\underline{r} - \underline{r}'| , \qquad (45)$$

where $\underline{r}'$ and $\underline{r}$ are the source point and field point, respectively.

Equation (44) states that the $\underline{E}$ field is given by the LHS for all field points outside the surface. On the other hand, for all field points <u>within</u> the surface the LHS vanishes identically, i.e. the surface field distributions must precisely cancel the incident wave. This latter statement is sometimes known as the extinction theorem, or the extended boundary condition.

The extinction theorem is applied to the curved fiber, shown in Fig. 20, as follows. Let a = fiber radius, and $\rho(s)$ = radius

of curvature as a function of position s along the axis of the fiber. We assume that

$$a/\rho_{min} < < 1 \tag{46a}$$

$$a/b < < 1 \tag{46b}$$

$$ka < < 1 , \tag{46c}$$

i.e., the fiber radius is much less than the minimum radius of curvature, the fiber half-length b, and free space wavelength $k = 2\pi/\lambda$, respectively. We also assume the fiber to have moderate to large conductivity, so that axial currents will be induced and guided along the fiber.

Now requiring that the <u>axial component</u> of Eq. (44) vanish <u>along the fiber axis</u> gives

$$(1/4\pi)\ \hat{s} \cdot \nabla \times \nabla \times \int d\sigma'\ i\hat{n}' \times \underline{H}_+(\underline{r}')\ g(kR)$$

$$+(1/4\pi)\ \hat{s} \cdot \nabla \times \int d\sigma'\ k\hat{n}' \times \underline{E}_+(\underline{r}')\ g(kR) = \hat{s} \cdot \underline{E}^{inc}(s) . \tag{47}$$

Note that this equation is still exact, although we have only used a portion of the information available. The curl operators may be taken under the integral sign, because the field point need never approach the fiber surface.

We suppose the magnetic field on the surface to be purely azimuthal, so that

$$\underline{H}_+ (\underline{r}') \equiv \hat{\phi}' H(s') ,$$

$$n' \times \underline{H}_+ (\underline{r}') = \hat{s}' H(s') . \tag{48}$$

Using the identity curl curl = grad div − div grad, the first integrand of Eq. (47) takes the form

$$\hat{s} \cdot \nabla \times \nabla \times \hat{n}' \times \underline{H}_+ (\underline{r}') \, g(kR) = \hat{s} \cdot (\nabla \nabla \cdot - \nabla \cdot \nabla) \hat{s}' H(s') \, g(kR)$$

$$= H(s') \, \hat{s} \cdot \nabla \nabla \cdot \hat{s}' \, g(kR) + k^2 (\hat{s} \cdot \hat{s}') H(s') \, g(kR)$$

$$= H(s') \, (\hat{s} \cdot \nabla) \, (\hat{s}' \cdot \nabla) \, g(kR) + k^2 \, (\hat{s} \cdot \hat{s}') \, H(s') \, g(kR)$$

$$= -H(s') \, [\partial^2 / \partial s \partial s' - k^2 \, (\hat{s} \cdot \hat{s}') \, g(kR) , \tag{49}$$

where in the last step we have used the formal notation $\hat{s} \cdot \nabla \equiv \partial / \partial s$ and $\hat{s}' \cdot \nabla \equiv -\partial / \partial s'$ for directional derivatives. The minus sign arises in the latter case because the primary variable has the form

$$\underline{R} = \underline{r}(s) - \underline{r}(s')$$

For the second integral of Eq. (47), the electric field on the surface is assumed to be purely axial, i.e.

$$\underline{E}_+(\underline{r}') = \hat{s}'\, E(s') \ . \tag{50}$$

Now

$$\begin{aligned}
\hat{s} \cdot \nabla \times \hat{n}' \times \underline{E}_+(\underline{r}')\, g(kR) &= -\hat{s} \cdot (\hat{n}' \times \underline{E}_+) \times \nabla g \\
&= (\hat{n}' \times \underline{E}_+) \cdot (\hat{s} \times \nabla g) \\
&= E(s')\, (\hat{n}' \times \hat{s}') \cdot (\hat{s} \times \nabla g) \\
&= -E(s')\, (\hat{s} \cdot \hat{s}')\, (\hat{n}' \cdot \nabla g) \\
&= -E(s')\, (\hat{s} \cdot \hat{s}')\, (\hat{n}' \cdot R) kg' \ , \\
&= -E(s')\, (\hat{s} \cdot \hat{s}')\, (a/R) kg' \ . \qquad (51)
\end{aligned}$$

Here in the fourth step we used the identity

$$(\underline{a} \times \underline{b}) \cdot (\underline{c} \times \underline{d}) = (\underline{a} \cdot \underline{c})\, (\underline{b} \cdot \underline{d}) - (\underline{a} \cdot \underline{d})\, (\underline{b} \cdot \underline{c})$$

then noted that the scalar product $\hat{n}' \cdot \hat{s}$ vanishes identically under the azimuthal portion of the surface integration. In the last step above $g'(kR) \equiv dg/d(kR)$ and we have assumed that

$$\hat{n}' \cdot \hat{R} = a/R \ . \tag{52}$$

Note from Fig. 20 that this equality only holds when $|s-s'| \ll \rho$, *i.e.*, for points sufficiently close together along the axis that

the curvature of the fiber has not come into play. No approximation is involved here, however, because the integral is entirely negligible otherwise, as we will now see.

Using Eq. (51), the second term of Eq. (47) becomes

$$-(k^2/4\pi) \int_0^{2\pi} a\,d\emptyset' \int_{-b}^{+b} ds'\ E(s')(\hat{s}\cdot\hat{s}')\ (a/R)\ g'(kR)$$

$$= -(k/2)\ (ka)^2 \int_{-b}^{+b} ds'\ E(s')(\hat{s}\cdot\hat{s}')\ (1/kR)\ g'(kR)$$

$$\approx (1/2)a^2\ E(s) \int_{-\infty}^{+\infty} ds'[(s-s')^2 + a^2]^{-3/2} = E(s)\ . \qquad (53)$$

From the first step one notes that because $ka \ll 1$ only that portion of the integral of order $(1/ka)^2$ will contribute to the final result. Noting that

$$(1/kR)\ g'(kR) \approx -(1/kR)^3 = -(1/k)^3\ [(s-s')^2 + a^2]^{-3/2}\ ,$$

for $kR \ll 1$, the remaining steps of Eq. (53) are straightforward.

Putting the results of Eqs. (49) and (53) back in Eq. (47) and carrying out the azimuthal integration, one finds that

$$(ia/2)\int_{-b}^{+b} ds'H(s')[\partial^2/\partial s\,\partial s' - k^2(\hat{s}\cdot\hat{s}')]g(s,s') - E(s)$$

$$= -\hat{s}\cdot\underline{E}^{inc}(s) \,. \tag{54}$$

We can express this result as an integral equation for <u>total line current</u> I(s) by writing

$$I(s) = 2\pi a i\, H(s) \,, \tag{55}$$

and introducing a surface impedance per unit length given by[4]

$$Z = -(\omega\mu/2\pi a k_f)\, J_o(k_f a)/J_o'(k_f a) \,. \tag{56}$$

Here $k_f = (\omega^2\mu\varepsilon + i\omega\mu\sigma)^{1/2}$ is the complex propagation constant within the fiber, J_o is the Bessel function of the first kind, and we have assumed that both E and H within the fiber vary much more rapidly in the radial than the axial direction. This assumption is consistent with the requirement of moderate to large conductivity. Note, however, that if one were to represent I(s) as a Fourier expansion, then eventually the axial variations

of such terms would dominate, with the result that k_f in Eq. (56) would have to be modified.[4] That is, the surface impedance becomes dependent on the rate of axial variation of current when that rate is large.

The tangential E field can now be expressed as

$$E(s) = ZI(s) \ , \tag{57}$$

and using this result, along with Eq. (55), one finally obtains

$$(1/4\pi) \int_{-b}^{+b} ds' \ I(s') \ [\partial^2/\partial s \ \partial s' - k^2(\hat{s}\cdot\hat{s}')] \ g(s,s') - ZI(s)$$

$$= -\hat{s} \cdot \underline{E}^{inc}(s) \ . \tag{58}$$

Note that for straight fibers $\hat{s}\cdot\hat{s}' = 1$ and this equation reduces to the usual formula.[3] Also, for curved, perfectly conducting wires $Z \longrightarrow 0$ and one again finds the accepted formula.[15]

4.3 Approximation for Special Fibers

For the general case, as described by the integral Eq. (58), it is clear that detailed numerical computations are required in order to obtain any explicit results. If the fiber axis has

radius of curvature large compared to wavelength, or is made up of a zigzag series of straight line segments, however, then the absorption cross-section is readily approximated using earlier results.

First, consider the case where the fiber axis curves only slowly and is relatively long, compared with wavelength. Then we can use the infinite cylinder result to obtain the absorption cross-section per unit length σ_a/ℓ, where this ratio is given by Eq. (30). Note that σ_a will be a function of position s along the curved fiber, in that σ_a depends on the angle θ_o formed by the incident E vector and the local tangent to the fiber axis. The <u>total</u> absorption cross-section Σ_{abs} is then given by

$$\Sigma_{abs} = \int_{-b}^{+b} ds \, [\sigma_a (s)/\ell] \, . \tag{59}$$

It is now straightforward to obtain results for toroidal or C-shaped fibers, or other configurations meeting the slowly-curving limitation, by numerical integration of Eq. (59).

For a fiber made up of zigzag line segments, it is more appropriate to emply the quasi-static approximation to the absorption cross-section σ_{abs} as given by Eq. (18). We have already seen by comparison with other computations that this formula is quite accurate for all fiber lengths provided the modified depolarization factor L' of Eq. (29) is used for $k_o \ell > 1$.

Now for a fiber of N segments, having individual lengths ℓ_n, n = 1, 2, ... , N, the total absorption cross-section Σ_{abs} is given simply by

$$\Sigma_{abs} = \sum_{n=1}^{N} \sigma_{abs} (\ell_n) \sin^2 \theta_n , \qquad 60)$$

where the factor $\sin^2\theta_n$ (angle between incident E vector and nth segment axis) is included because the original Eq. (18) was specifically for broadside incidence.

It is useful to note that for both Eqs. (59) and (6) the cross-section Σ_{abs} is a linear sum of the cross-sections of individual segments. Because each such segment behaves precisely *as a straight fiber under orientation averaging, one concludes* that the orientation-averaged cross-section $\overline{\Sigma}_{abs}$ for the curved fiber will be just equal to that of a straight fiber of the same total length.

5.0 TARGET OBSCURATION

In this section, taking into consideration both the diffuse cloud scattering properties and the beam extinction properties, one requires the optimum conditions for target obscuration from a mass efficiency standpoint, over a wavelength range where the theory is believed to be most accurate. It is appropriate to employ the quasistatic approximation, in which particles are assumed to be small in comparison with sensor wavelength.

Consider the situation when a target of (radar or optical) cross-section σ_T is partially concealed by a cloud of particles, the cloud having an incoherent cross-section Σ_c. Because of this incoherence, the cross-sections are additive and one has

$$\text{Observed cross-section} = \Sigma_c + \sigma_T \, e^{-2\gamma\tau} \quad , \tag{61}$$

where γ and τ are the decay constant and thickness of the cloud, respectively.

We now assume that the sensor <u>cannot</u> detect the target if

$$\Sigma_c \geq K\sigma_T \, e^{-2\gamma\tau} \tag{62}$$

where K is a figure of merit, e.g. for K = 0.1 the signal from the target would be 10 dB down in the "noise" of the cloud return. The diffuse scattering from the cloud has earlier been computed to be[5,6]

$$\Sigma_c = \frac{A_c}{\sqrt{3}} \left(\frac{k_o^2}{8\pi}\right) V_p \, \sigma_c' \quad , \tag{63}$$

where V_p is single-particle volume, the reduced conductivity is given by $\sigma_c' = k_o \varepsilon'' = \sqrt{\mu_o/\varepsilon_o}\, \sigma_c$ (in terms of conductivity, or the imaginary part of the relative dielectric constant), and A_c is the geometrical cross-section of the cloud, or the sensor beam cross-section at the cloud, if the latter should be smaller. Using this result, and taking the equality in Eq. (62) then gives

$$\frac{A_c}{\sqrt{3}} \left(\frac{k_o^2}{8\pi}\right) V_p \sigma_c' = K \sigma_T e^{-2\gamma\tau} \quad . \tag{64}$$

The decay constant for the cloud is given by

$$\gamma = \bar{n} \bar{\sigma}_{ext} \quad , \tag{65}$$

in terms of the number density of particles and the orientation-averaged extinction cross-section per particle. Assuming that absorption effects dominate, one has

$$\bar{\sigma}_{ext} \approx \bar{\sigma}_{abs} \approx \frac{\sigma_c' V_p}{3[1 + (L\varepsilon'')^2]} \approx \sigma_c' V_p/3 \tag{66}$$

where in the next-to-last step the quasistatic approximation was employed, and in the last step we noted that optimum absorption will occur when

$$L\varepsilon'' = 4(a/\ell)^2 [\, n(\ell/a) - 1] \varepsilon'' << 1 \tag{67}$$

(L is the depolarizing factor). Note also that the total mass M of particles can be written

$$M = \rho V_p \bar{n}\tau A_c \quad . \tag{68}$$

Employing Eqs. (65), (66) and (68) in Eq. (64), and taking the logarithm of the result determines the required mass to be

$$M = \frac{3\rho A_c}{2\sigma_c'} \ell n \left[\frac{8\sqrt{3}\,\pi}{k_o^2 V_p \sigma_c'} \left(\frac{K\sigma_T}{A_c} \right) \right] . \qquad (69)$$

The quantities K, σ_T and A_c are prescribed by the logistics of the task at hand. Thus, to minimize M one first must seek a material with smallest possible value of the ratio ρ/σ_c'. In addition, it is desirable to obtain as large a value of the product $k_o^2 V_p \sigma_c'$ as possible, in order to minimize the logarithmic term in Eq. (69).

For concreteness, suppose that

$$L\varepsilon'' = 0.1 ,$$

$$k_o \ell = 0.1 . \qquad (70)$$

From Eq. (67) we then find that

$$a = \frac{0.01\ (\ell/a)}{4\ \sigma_c'\ [\ell n(\ell/a) - 1]} . \qquad (71)$$

This equation can be used to determine particle radius, once the length and conductivity are known. Typical particle design parameters can now be listed:

a) <u>microwave region</u>

$\gamma = 3.\times 10^{-2}$ m

$\ell = 4.8 \times 10^{-4}$ m

$\sigma_c = 5 \times 10^{6}$ mho/m

$a = 2.2 \times 10^{-8}$ m

b) <u>infrared region</u>

$\gamma = 3 \times 10^{-5}$ m

$\ell = 4.8 \times 10^{-7}$ m

$\sigma_c = 1 \times 10^{4}$ mho/m

$a = 1.0 \times 10^{-8}$ m

6.0 TAILORING OF PARTICLE PARAMETERS FOR SPECIFIC APPLICATIONS

It is the purpose of this section to demonstrate the techniques by which the parameters (length, radius, and conductivity) of thin conductive fibers can be adjusted so that a cloud of these particles will have selected specified spectral characteristics. These characteristics are: (1) large absorption and small scattering, (2) large scattering and low absorption, and (3) transparency. Two frequencies were arbitrarily chosen for the cases to be analyzed. These are $f_1 = 10^{10}$ Hz and $f_2 = 10^{12}$ Hz, corresponding to wavelengths of 3 cm (microwave) and 300 microns (infrared).

The analyses to be discussed will be based on our "extended quasistatic model", the basis of which is described in Section 2.2. As demonstrated in Section 3, this analytical model produces

results which are in surprisingly good agreement with the results obtained using the much more rigorous variational technique of Section 2.1. To be more explicit, the quasistatic model can be used to calculate the absorption cross section over a very wide range of $k_o\ell$, including $k_o\ell >> 1$. The scattering cross section computations resulting from the quasistatic model are valid only in the range $k_o\ell \leq \pi$.

In all of the cases analyzed, the results of the quasistatic calculations are directly compared with the corresponding results of the variational technique. We find these comparisons to be quite remarkable.

6.1 Constitutive Equations

In addition to the equations of Sections 2.2, 2.4 and 2.5, the following equations are utilized in the foregoing analyses:

Orientation-averaged absorption cross-section (see Eq. 21):

$$\bar{\sigma}_{abs} = \left(\frac{1}{3}\right) \sigma_{abs} \tag{72}$$

Orientation-averaged scattering cross-section (see Eq. 22):

$$\bar{\sigma}_{sca} = \left(\frac{1}{5}\right) \sigma_{sca} \tag{73}$$

High frequency depolarizing factor (see Eq. 29):

$$L' = 4 \left(\frac{k_o a}{\pi}\right)^2 \left[\ell n \left(\frac{\pi}{k_o a}\right) - 1 \right] \quad (k_o \ell \leq \pi) \tag{74}$$

The inclusion of the above equation permits extension of the calculation of absorption cross section well into the $k_o \ell >> 1$ regime. Due to this, we refer to the present theory as the "extended quasistatic theory."

In this treatment, we are using the Drude (free electron) model for the complex dielectric constant (Section 2.4) and the Fuchs model for the dependence of conductivity on particle dimensions, and we have purposely chosen frequencies ω_1 and ω_2 such that possible anomalies due to these do not appear. Also, for purposes of analysis, we can make the simplification $\varepsilon = i\varepsilon''$. The computer program, however, does not utilize this simplification.

6.2 Absorb at 3 cm, Reflect at 300 microns

These criteria lead to the following mathematical statements:

At frequency $\omega_1 = 2\pi \times 10^{10}$ Hz

$$\frac{\bar{\sigma}_{sp\ (1)}}{\bar{\sigma}_{sp\ (2)}} << 1 \tag{75}$$

Let $$\frac{\bar{\sigma}_{sp\ (1)}}{\bar{\sigma}_{sp\ (2)}} = .01 \tag{76}$$

$$(L\varepsilon''\ (1))^2 << 1 \tag{77}$$

Let $$L\varepsilon''\ (1) = 0.1 \tag{78}$$

Equation (7) ensures that the absorption cross section will be at its maximum value at frequency ω_1, but will be reduced by a large factor at frequency $\omega_2 = 2\pi \times 10^{12}$ Hz. Also, we know that the scattering cross section will be at least as great at ω_2 as at ω_1. This will cause $\sigma_{sca}(2)/\sigma_{abs}(2)$ to be large, which is what we seek at ω_2.

From Eqs. (76), (78), (72), and (73), we obtain (with the appropriate definitive equations of Section 2.2) equations for the conductivity σ_c, radius a and length ℓ:

$$\sigma_c = \frac{\varepsilon_o c^2 (.03)^{2/3}}{\omega_1 \, a^2 \, \{10 \, [\ell n \, (\frac{\ell}{a}) - 1]\}^{1/3}} \quad , \tag{79}$$

$$a = \frac{c \, (.03)^{1/3} \, (\varepsilon_o)^{1/2}}{(\omega_1)^{1/2} \{10 \, [\ell n \, (\frac{\ell}{a}) - 1]\}^{1/6} (\sigma_c)^{1/2}} \tag{80}$$

$$\ell = 2a \left\{10 \, [\ell n \, (\frac{\ell}{a}) - 1] \, \left(\frac{\sigma_c}{\omega_1 \, \varepsilon_o}\right)\right\}^{1/2} \tag{81}$$

when Eqs. (79) and (80) are equivalent, i.e., we can choose a conductivity and solve for a, or choose a radius, a, and solve for the conductivity σ_c. We will do the former. Knowing both a and σ_c, we then calculate the length from (81). Note that the term in square brackets in (79), (80), and (81) is very insensitive to large variations in (ℓ/a). This is especially true when it is raised to fractional powers in (79) and (80). Therefore, we can come quite close to the desired results if we simply let [ ] = 2.5. This permits direct estimation of a and ℓ, given a preselected value of σ_c.

Table I

Cond =	1.00E+04	Radius =	8.68E-06
Length =	3.71E-03	$k_0(1)\,\ell/2$ =	3.88E-01
Cond =	1.00E+05	Radius =	2.75E-06
Length =	3.71E-03	$k_0(1)\,\ell/2$ =	3.88E-01
Cond =	1.00E+06	Radius =	8.68E-07
Length =	3.71E-03	$k_0(1)\,\ell/2$ =	3.88E-01
Cond =	1.00E+07	Radius =	2.75E-07
Length =	3.71E-03	$k_0(1)\,\ell/2$ =	3.88E-01
Cond =	1.00E+08	Radius =	8.68E-08
Length =	3.71E-03	$k_0(1)\,\ell/2$ =	3.88E-01
Cond =	1.00E+09	Radius =	2.75E-08
Length =	3.71E-03	$k_0(1)\,\ell/2$ =	3.88E-01

The above procedure leads to sets of permissible parameter values, as exemplified in Table I. Substitution of the various parameter sets into the computer program yields graphs such as shown in Fig. 21. Since these graphs are identical over the wavelength range 300 microns to 3 cm, only one is shown. This figure is representative of a fairly highly conducting metal (bulk conductivity = 10^7 mho/m). The relaxation time τ is that of copper.

From Fig. 21, we see that (1) indeed, the absorption cross section peaks at very nearly the wavelength λ_1 = 3 cm, (2) that, in the case of absorption, the extended quasistatic theory is in excellent agreement with the variational theory for wavelengths greater than about 50 microns, and (3) the scattering as calculated from both theories is in excellent agreement when $k_0\ell \lesssim 1$.

We further conclude that the mathematical "design" procedure demonstrated in this sub-section, although not analytically exact, provides good parametric sets for the solution of the stated problem, since the objectives are met at the two specified wavelengths.

6.3 Absorb at 3 cm, Absorb at 300 microns

We have quite different criteria for this problem as compared with the preceding problem. Here, we wish to have a very highly absorbing cloud which has low scattering cross section.

In this case, the cloud scattering cross section Σ_c is given by

$$\Sigma_c = A_c \left(\frac{\bar{\sigma}_{sca}}{2\,\bar{\sigma}_{abs}}\right) \quad , \tag{82}$$

where A_c = projected area of the cloud or that portion thereof which occupies the solid angle of the incident beam.

Obviously, we wish to make the absorption cross section of the particle much larger than its scattering cross section. This must be true over at least the wavelength range from 300 microns to 3 cm.

The above considerations lead to the following mathematical criteria:

(1) In order to have maximum absorption over the specified wavelength range, we want $L\varepsilon''(1) \ll 1$ and $L\varepsilon''(2) \ll 1$.

This means that the particles should be very thin and (perhaps) not too highly conducting.

(2) Since, under the above conditions, $\bar{\sigma}_{sca} \sim k_o^2 V_p^2 \sigma_c^2$ and $\sigma_{abs} \sim V_p \sigma_c$, the ratio $(\bar{\sigma}_{sca}/\bar{\sigma}_{abs})$ is proportional to $k_o^2 V_p \sigma_c$. Therefore, in order to maintain high cloud absorption and low cloud scattering, we wish to keep the product $V_p \sigma_c$ low (we have no control over k_o).

A little bit of experimenting with the extended quasistatic (EQ) computer program yields appropriate sets of parameters. The parameter set corresponding to minimal total mass is a = 100 Angstroms, ℓ = 100 microns, and $\sigma_c = 10^6$ mho/m as the bulk conductivity. The results of using these parameters in the EQ and variational codes are shown in Fig. 22. One can trade off a larger radius for a lower conductivity and achieve similar results, but with a somewhat higher ratio of $(\bar{\sigma}_{sca}/\bar{\sigma}_{abs})$.

Note again the remarkable agreement between the computations based on the two independent theories!

6.4 Reflecting Modes

It is easy to design particles having very low absorption and relatively high scattering. Experience has shown us that if, for example, we choose a highly conducting metal such as copper or aluminum, and select a radius of one micron or greater, the particle will be essentially completely reflecting for at least all wavelengths below 30 microns. We can tailor the scattering

cross section to become proportional to ω^4 at wavelengths significantly below that for which $k_o \tilde{=} 1$, which of course, represents Rayleigh scattering from "perfectly conducting" wires. Thus, the aggregate of particles can easily be made to be reflecting at one wavelength and essentially transparent at some (significantly) lower wavelength. Chaff clouds behave in this way.

6.5 Transparent at 3 cm, Absorb at 300 Microns

In this case, we want the scattering cross section to be much lower than the absorption cross section at all wavelengths under consideration. The requirements due to this and the transparency criterion at ω_1 are given below:

(1) Make $V_p \sigma_c$ as small as possible, consistent with the other criteria.

(2) Make $L\varepsilon'' = 1$ at ω_2.

(3) Make $k_o \ell < 1$ at ω_2.

Application of these criteria leads to the parameters listed in Figure 23. Note that, at $\lambda = 3$ cm, the absorption is three orders of magnitude lower than that at $\lambda = 300$ microns. The scattering throughout the ω_1 to ω_2 spectrum is much lower than the absorption.

6.6 Comments Relative to Particle Parameter Tailoring

(1) Our extended quasistatic treatment provides a very useful tool in the design of particles for specified applications. In some instances, the e.q.s. theory does not yield accurate quantitative data and should be used primarily as a first step to be followed by the full computation using our Variational method.

(2) The calculation of <u>scattering</u> cross sections using the EQ theory is limited to the range $k_o \ell / 2 \leq 1$. Unfortunately, the accuracy of the scattering cross sections using the variational theory decreases substantially for $k_o \ell >> 1$. This is discussed in Section 3. Our numerical integration technique is presently undergoing substantial improvement. Also, we are presently using the Hewlett Packard HP 9000, Model 520 computer for these calculations - providing much higher computation speed.*

(3) We have included backscatter cross section computations in Figures 21, 22 and 23 for those applications that require this.

(4) Within the bounds of present technology, it is possible to create particle parameters that could provide useful spectral characteristics over a wide wavelength range.

---

*Note - added in proof: At the time of submission of this report, we have made substantial improvements in our numerical integration routines. This includes $k_o \ell$ dependent incrementing of the number of the scattering cross section computations. The minimum incrementation of scattering angle is 0.05 deg. and the maximum is 1.0 deg. This gives good results for $k_o \ell \lesssim 350$.

REFERENCES

1. N. E. Pedersen, J. C. Pedersen and P. C. Waterman, Final Report on Theoretical Study of Single and Multiple Scattering by Cylinders, prepared for U. S. Army Chemical Systems Laboratory (September 27, 1984).

2. C. T. Tai, Electromagnetic backscattering from cylindrical wires, J. Appl. Phys., Vol. 23, pp. 909-916 (August, 1952).

3. E. S. Cassedy and J. Fainberg, Electromagnetic cross sections of finite conductivity wires, The Johns Hopkins Laboratory Technical Report No. AF-81, August 1960.

4. J. R. Wait, Exact surface impedance for a cylindrical conductor, Electr. Lett. 15, 659-660 (1979).

5. N. E. Pedersen and J. C. Pedersen, Theoretical, Experimental and Systems Studies on a New Technique for Radar Cross Section Reduction, AVCO RADTN-65-67, 8 December 1965.

6. N. E. Pedersen, J. C. Pedersen and H. A. Bethe, "A New Method of Radar Target Concealment," Proc. Tri-Service Radar Symposium, San Diego, 1969.

7. J. R. Wait, Scattering of a plane wave from a circular dielectric cylinder at oblique incidence, Can. J. Phys. 33, 189 (1955).

8. J. R. Wait, The long wavelength limit in scattering from a dielectric cylinder at oblique incidence, Can. J. Phys. 43, 2212 (1965).

9. M. A. Ordal et al., Appl. Optics 22, 1-99 (1983).

10. F. Wooten, Optical Properties of Solids (Academic Press, New York, 1972).

11. K. Fuchs, Proc. Camb. Phil. Soc. 34, 100 (1938).

12. R. B. Dingle, Proc. Roy. Soc. A201, 545 (1950).

13. C. Kittel, Introduction to Solid State Physics (Wiley, New York, 1956), Chap. 10.

14. J. Aharoni, Antennae - An Introduction to Their Theory (Clarendon Press, Oxford, 1946) pp. 133-135.

15. K. K. Mei, IEEE Trans. Ant. Prop. AP-13, 374 (1965).

16. R. G. Kouyoumjian, Appl. Sci. Res. B6, 165 (1956).

17. L. L. Philipson, IRE Trans. Ant. Prop, 6, 3 (1958).

18. C. Acquista, Effects of axis wander on scattering by thin tenuous cylinders, Proc. 1980 Chemical Systems Laboratory Scientific Conference on Obscuration and Aerosol Research (June 1983), p. 17.

19. P. C. Waterman, Phys. Rev. D 3, 825 (1971).

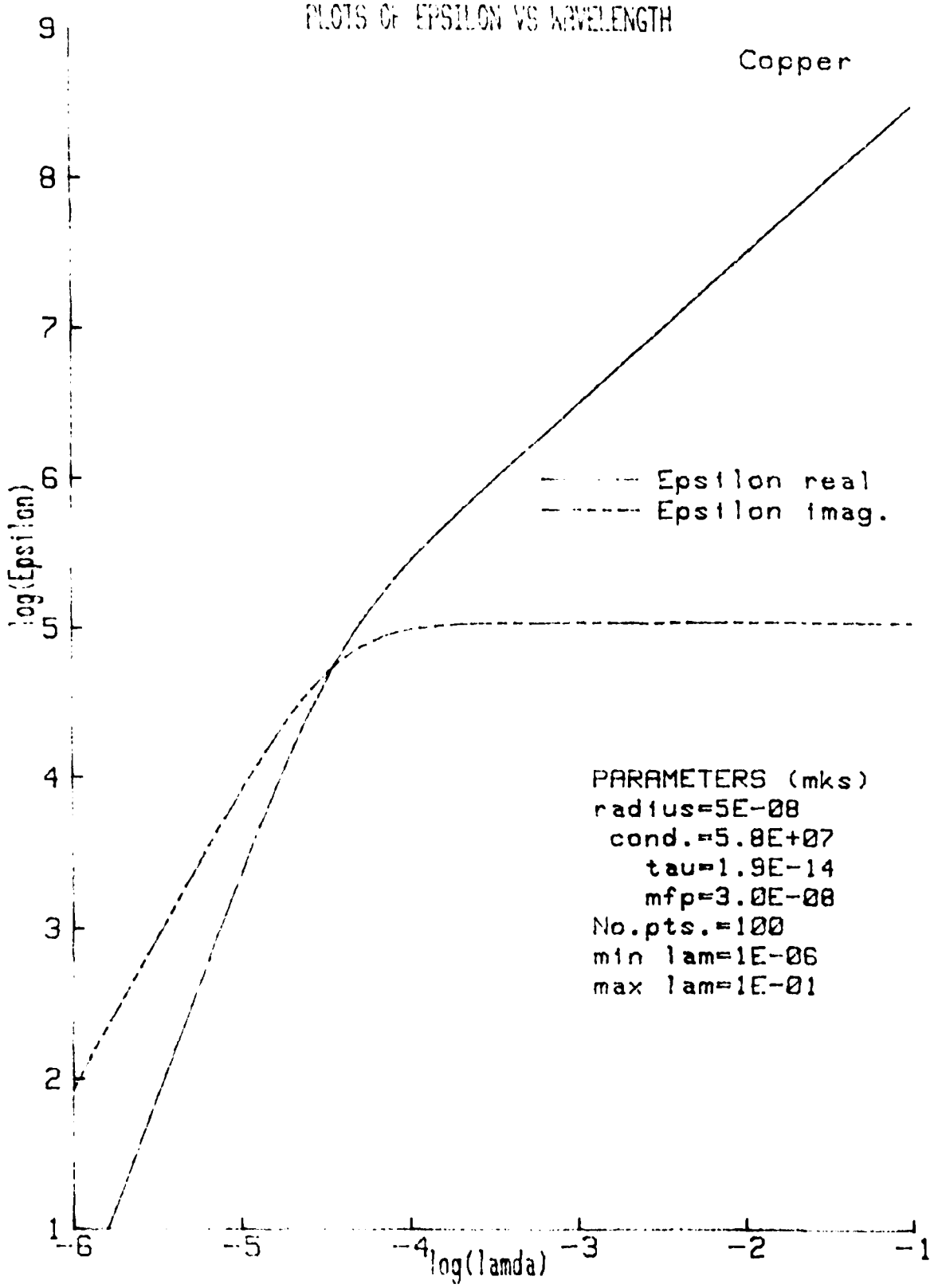

Fig. 1. Complex dielectric constant vs. wavelength for copper.

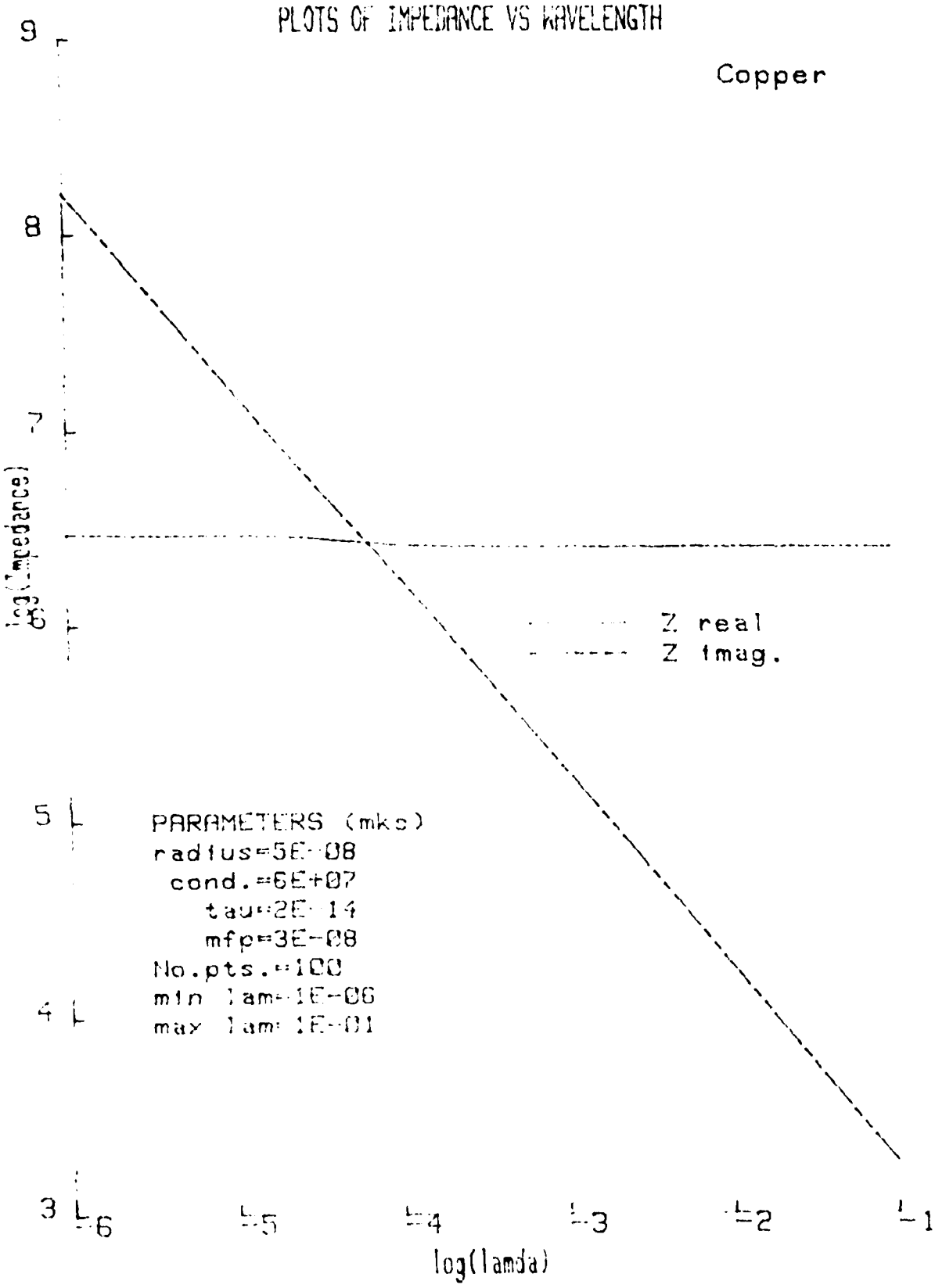

Fig. 2. Complex surface impedance vs. wavelength for copper.

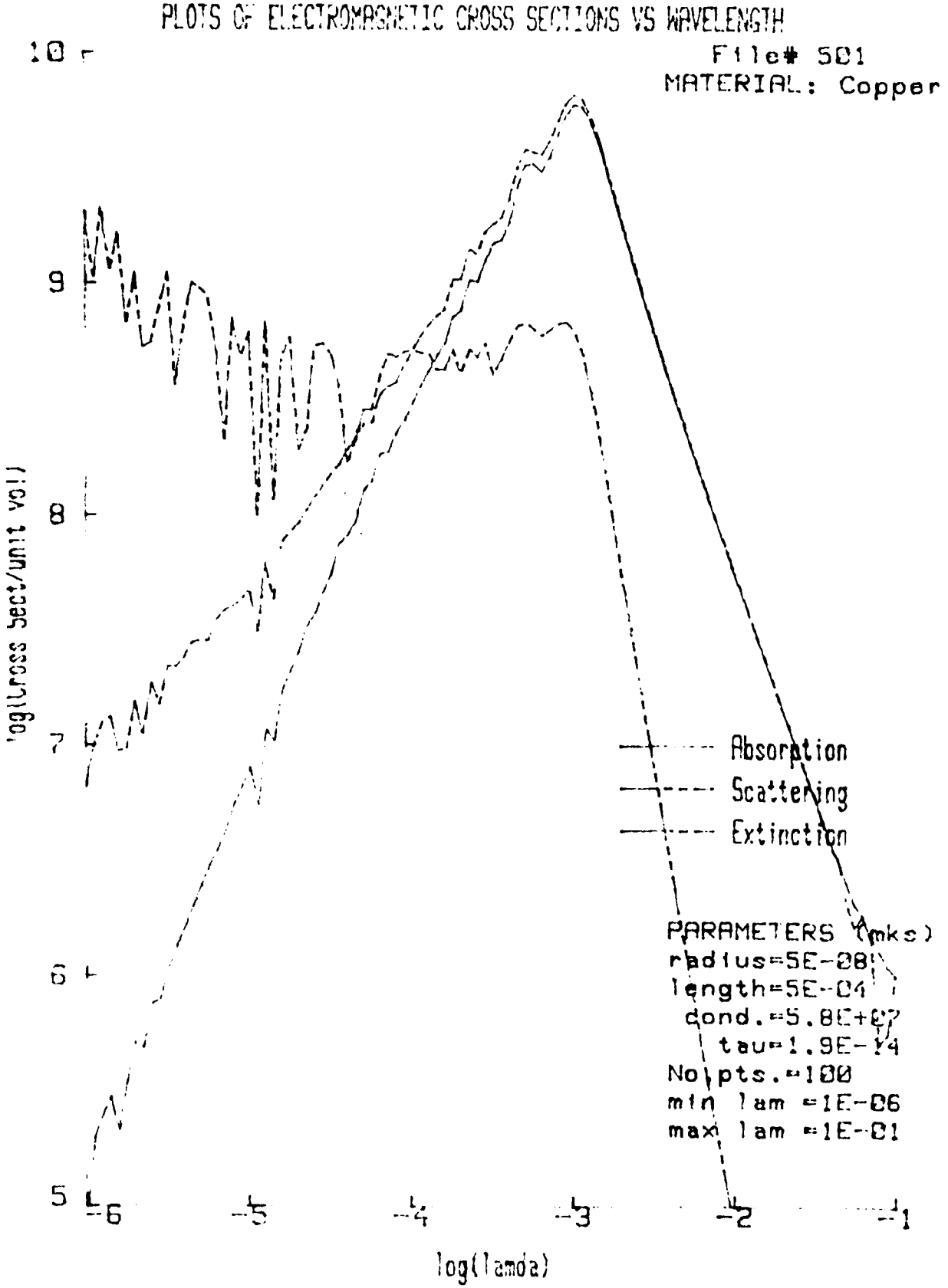

Fig. 3. Cross-sections vs. wavelength for copper (variational method).

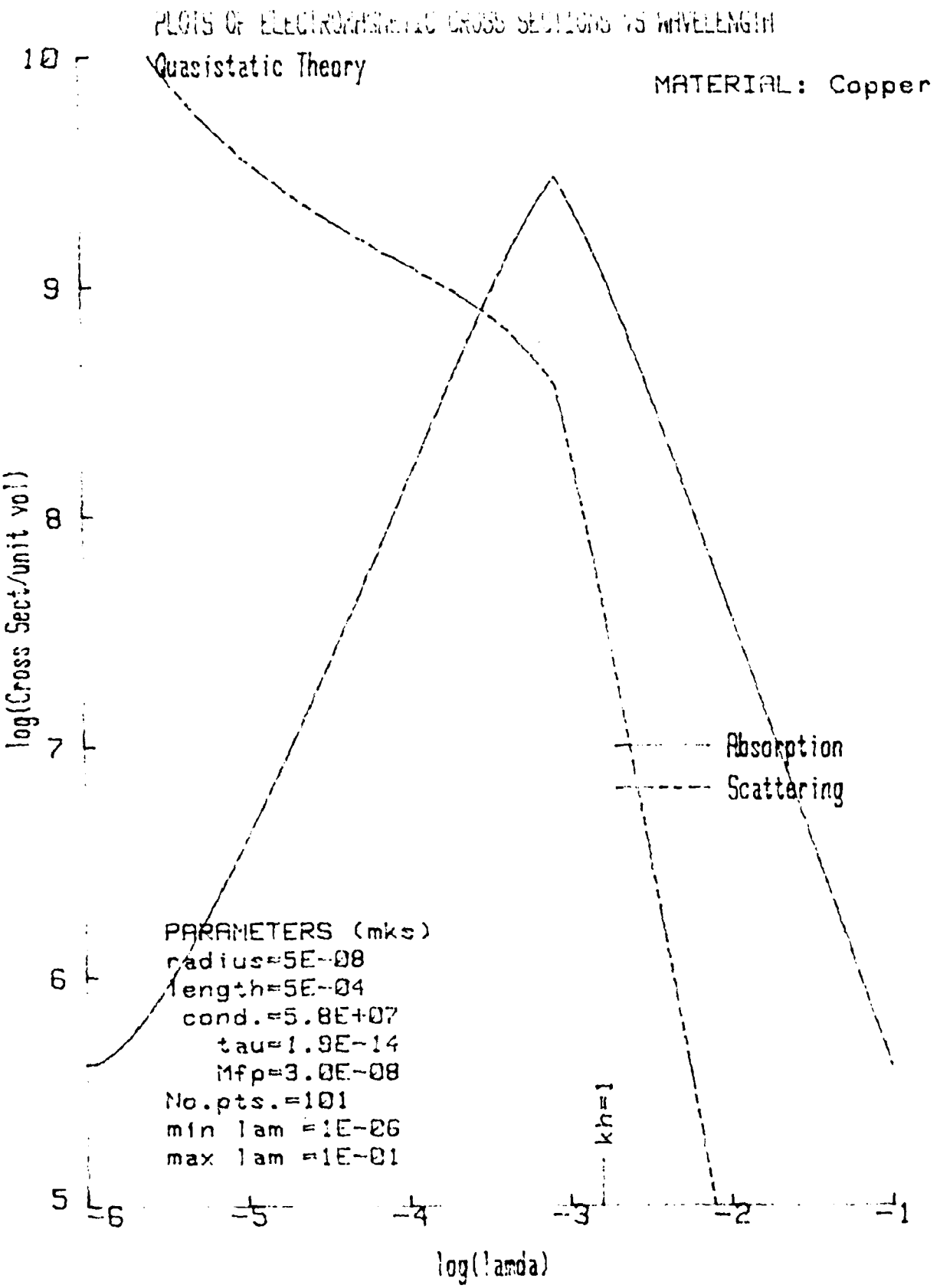

Fig. 4. Cross-sections vs. wavelength for copper (quasistatic theory).

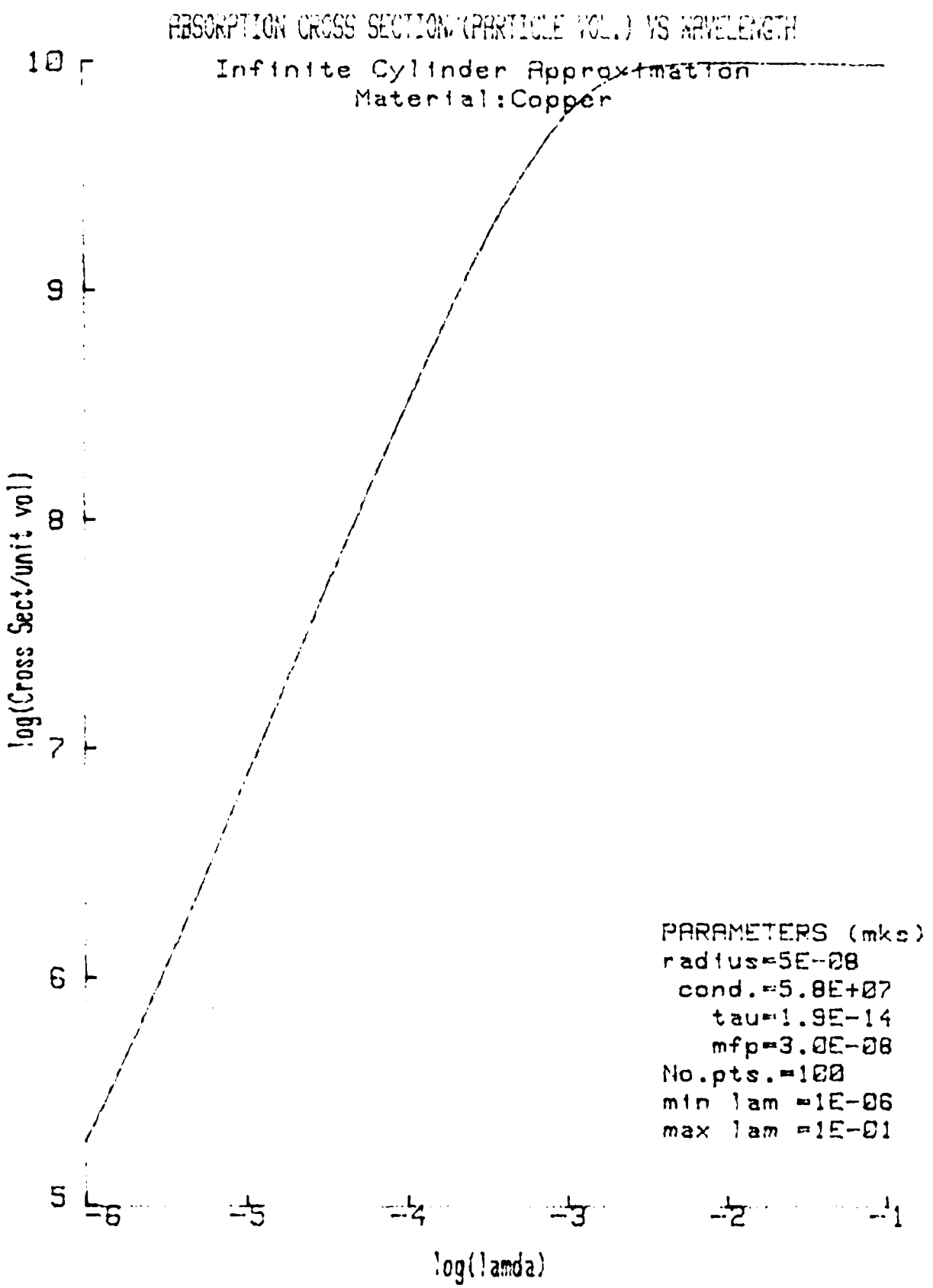

Fig. 5. Absorption cross-section vs. wavelength for copper (infinite cylinder approximation).

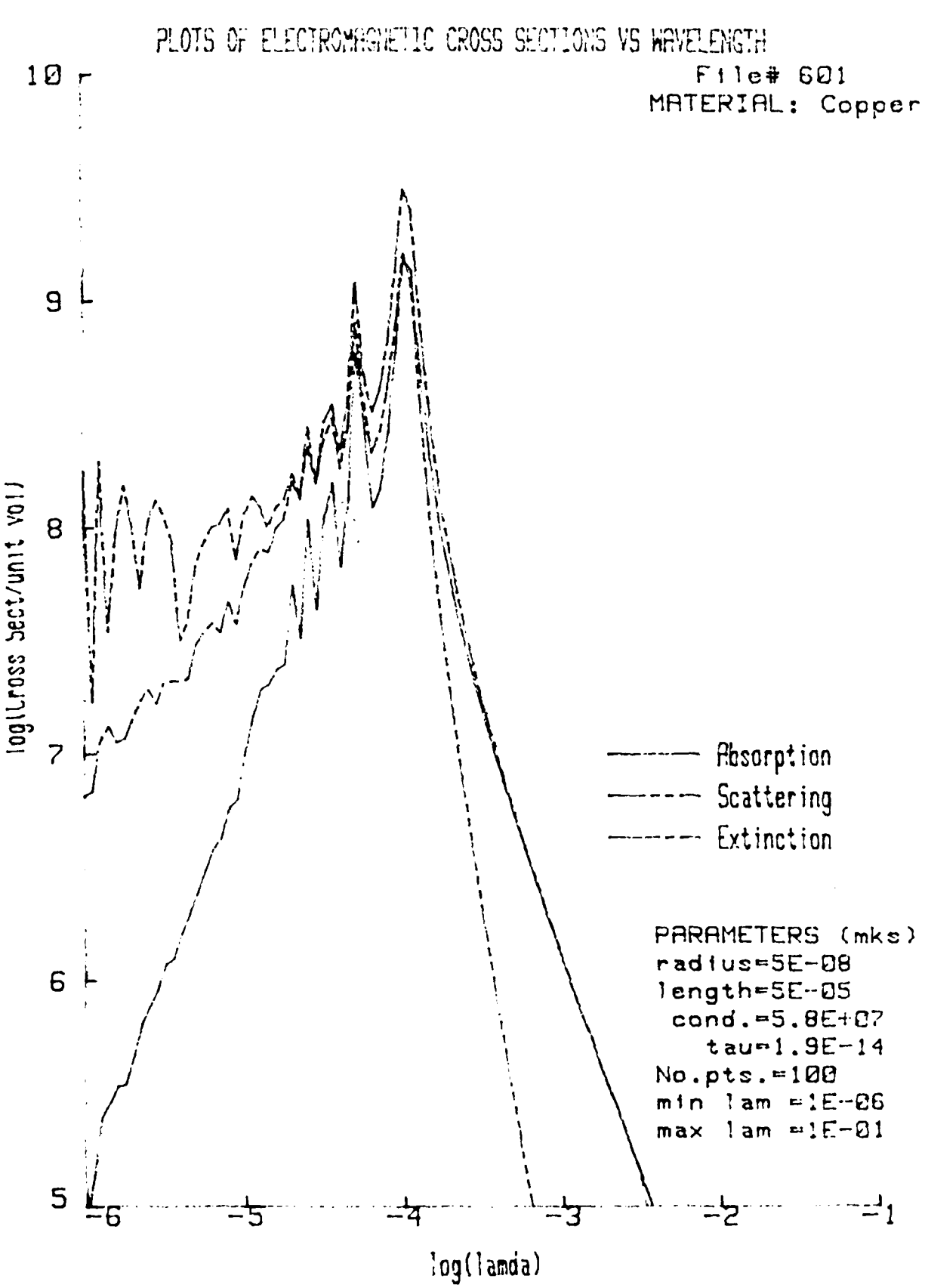

Fig. 6. Cross-sections vs. wavelength for copper (variational method).

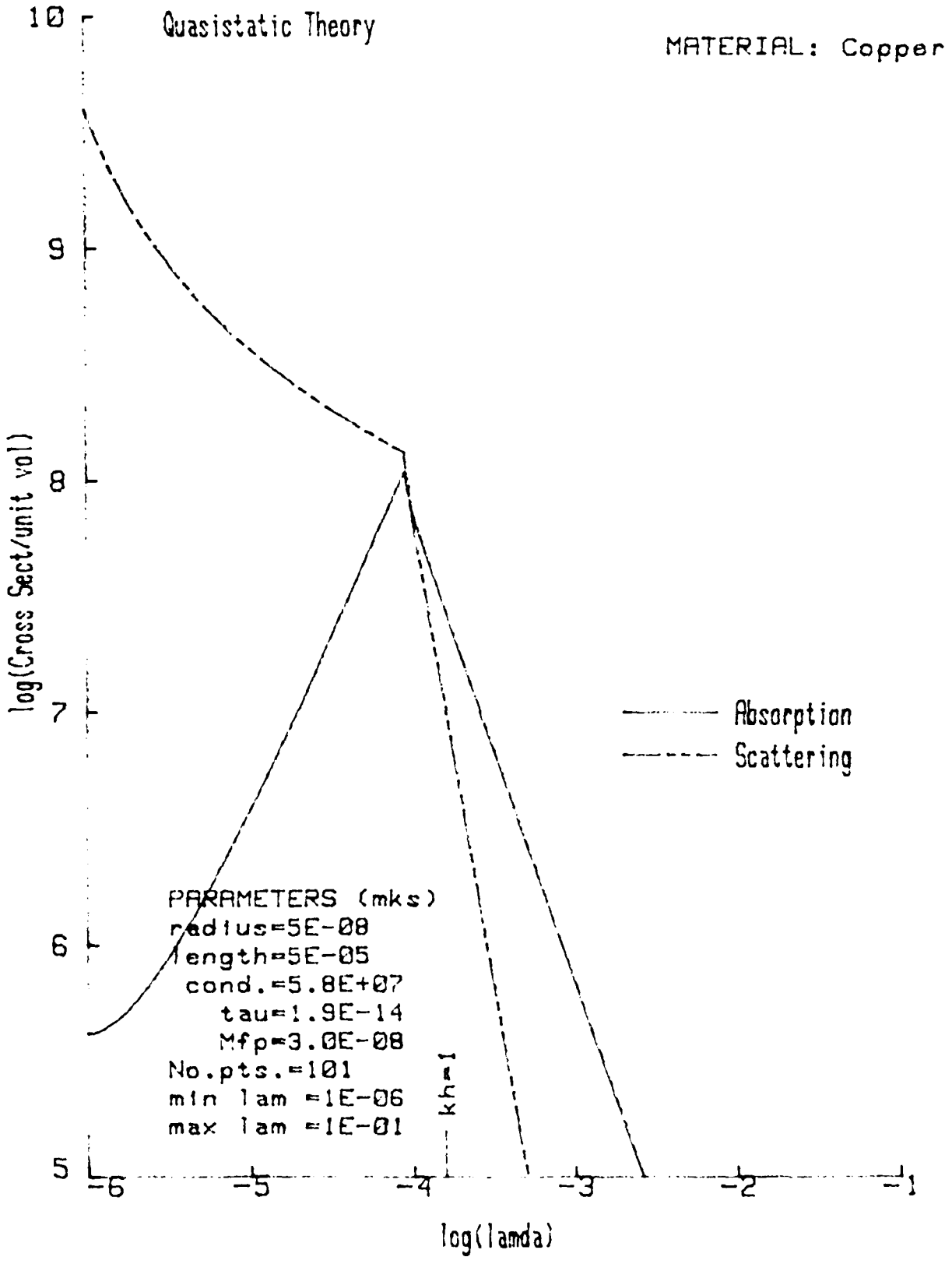

Fig. 7. Cross-sections vs. wavelength for copper (quasistatic theory).

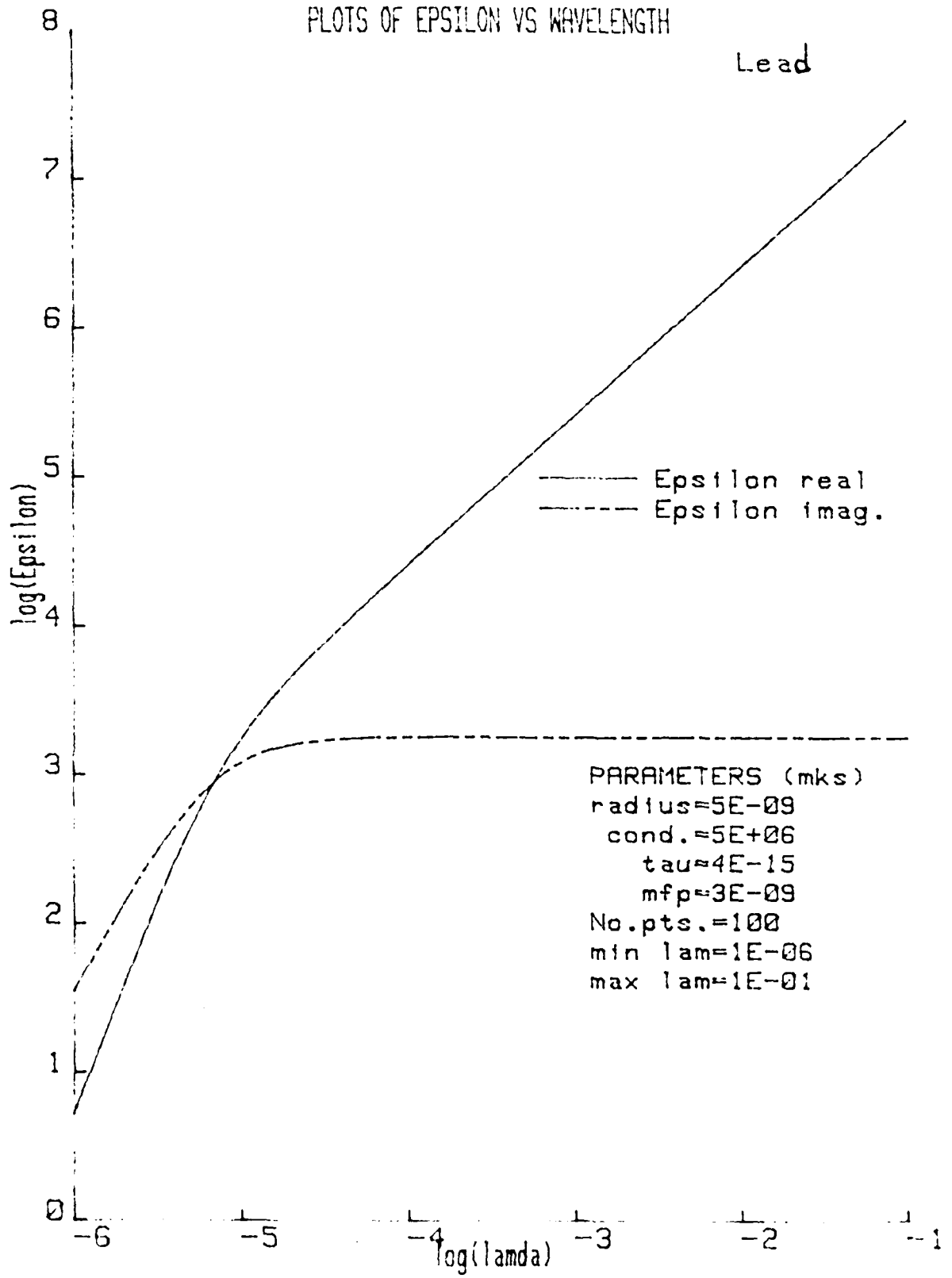

Fig. 8. Complex dielectric constant vs. wavelength for lead.

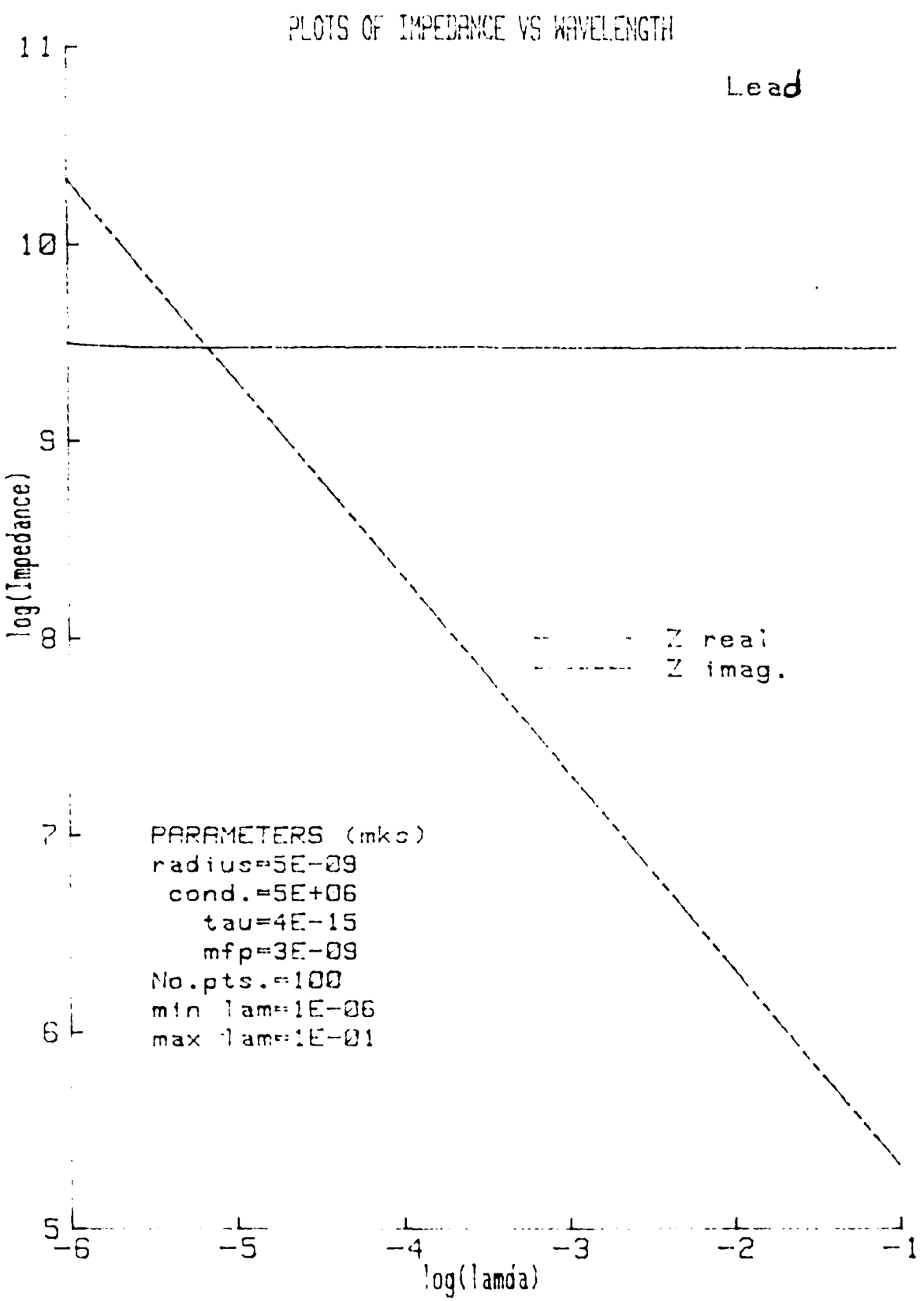

Fig. 9. Complex surface impedance vs. wavelength for lead.

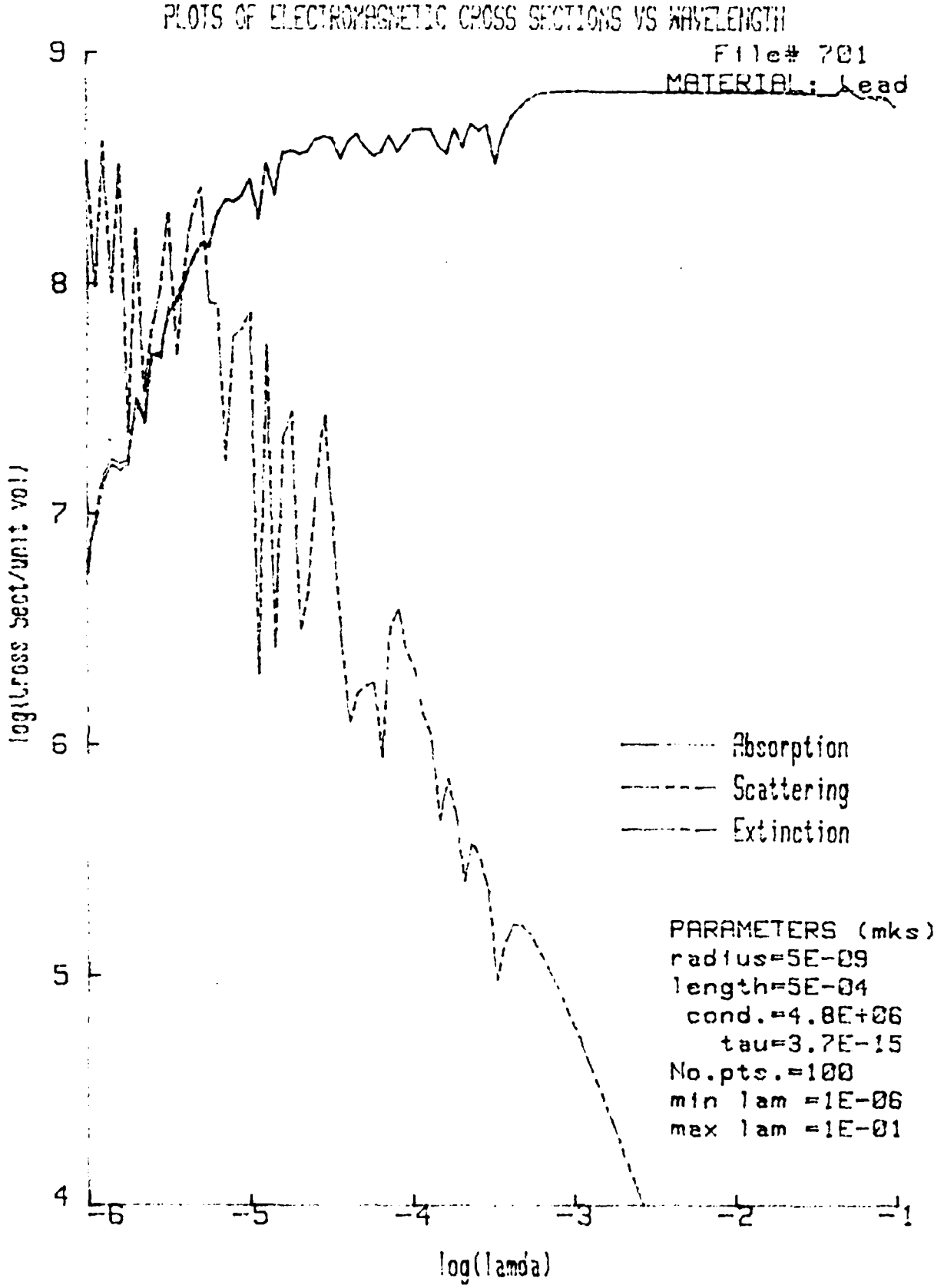

Fig. 10. Cross-sections vs. wavelength for lead (variational method).

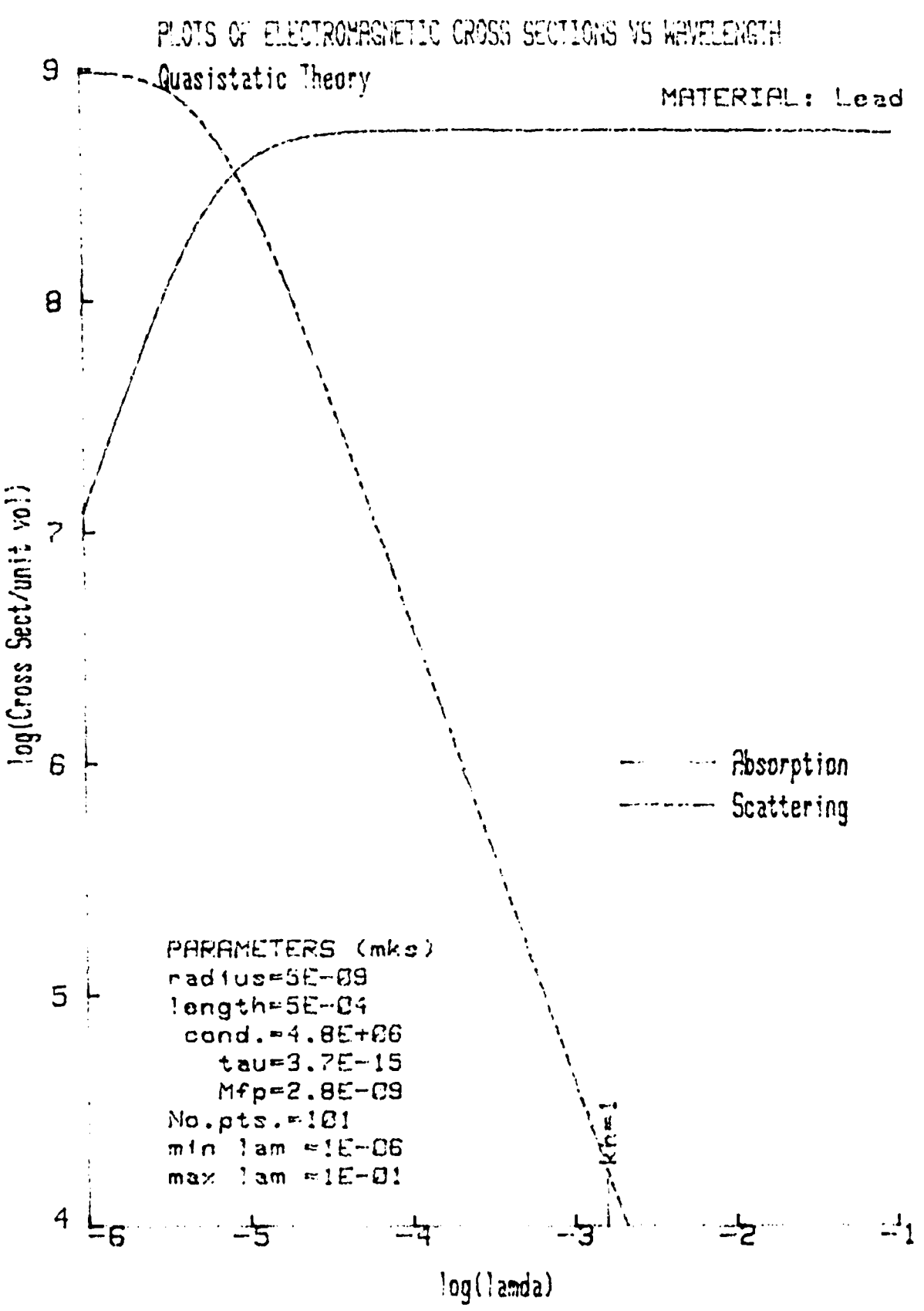

Fig. 11. Cross-sections vs. wavelength for lead (quasistatic theory).

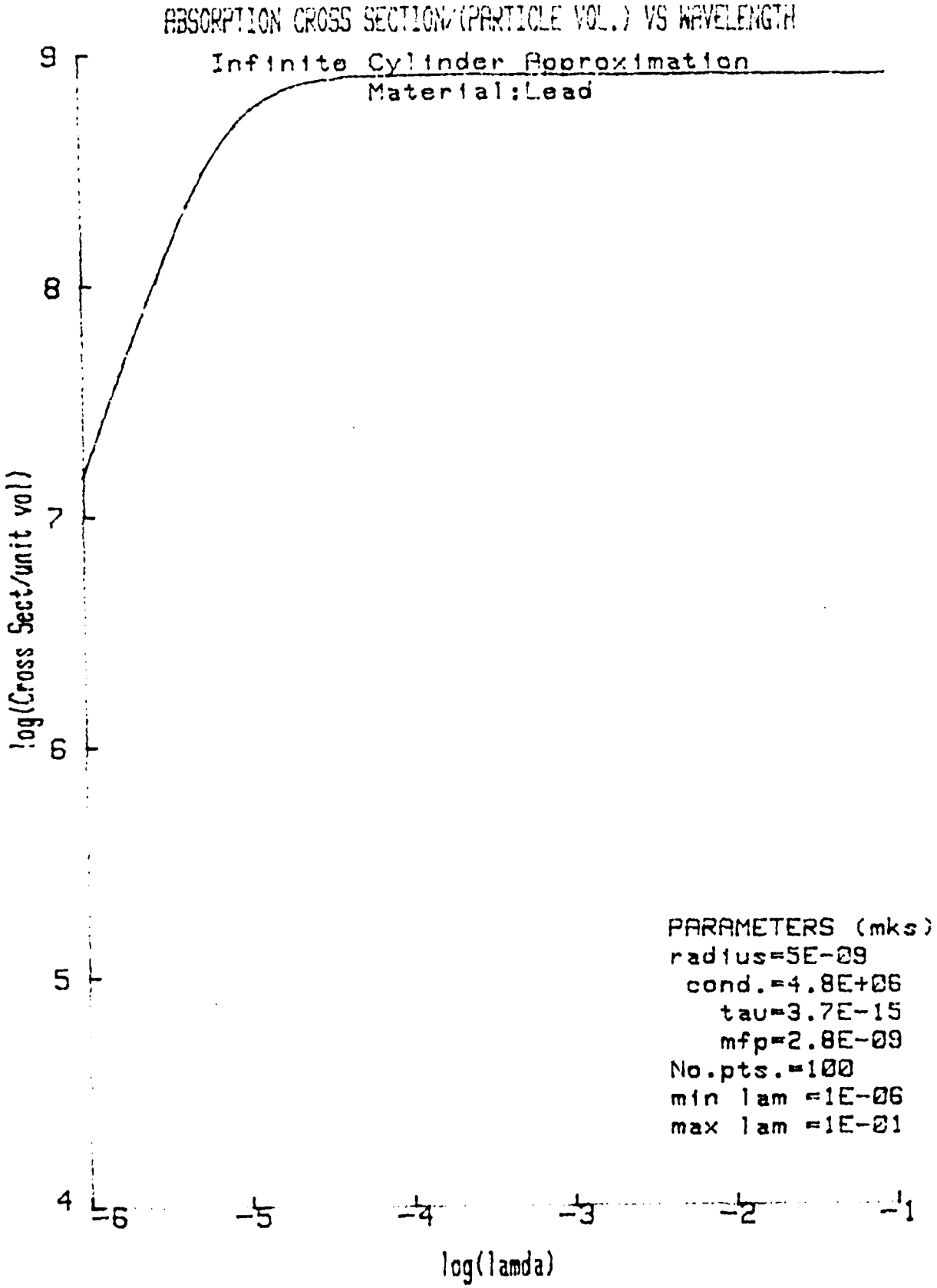

Fig. 12. Absorption cross-section vs. wavelength for lead (infinite cylinder approximation).

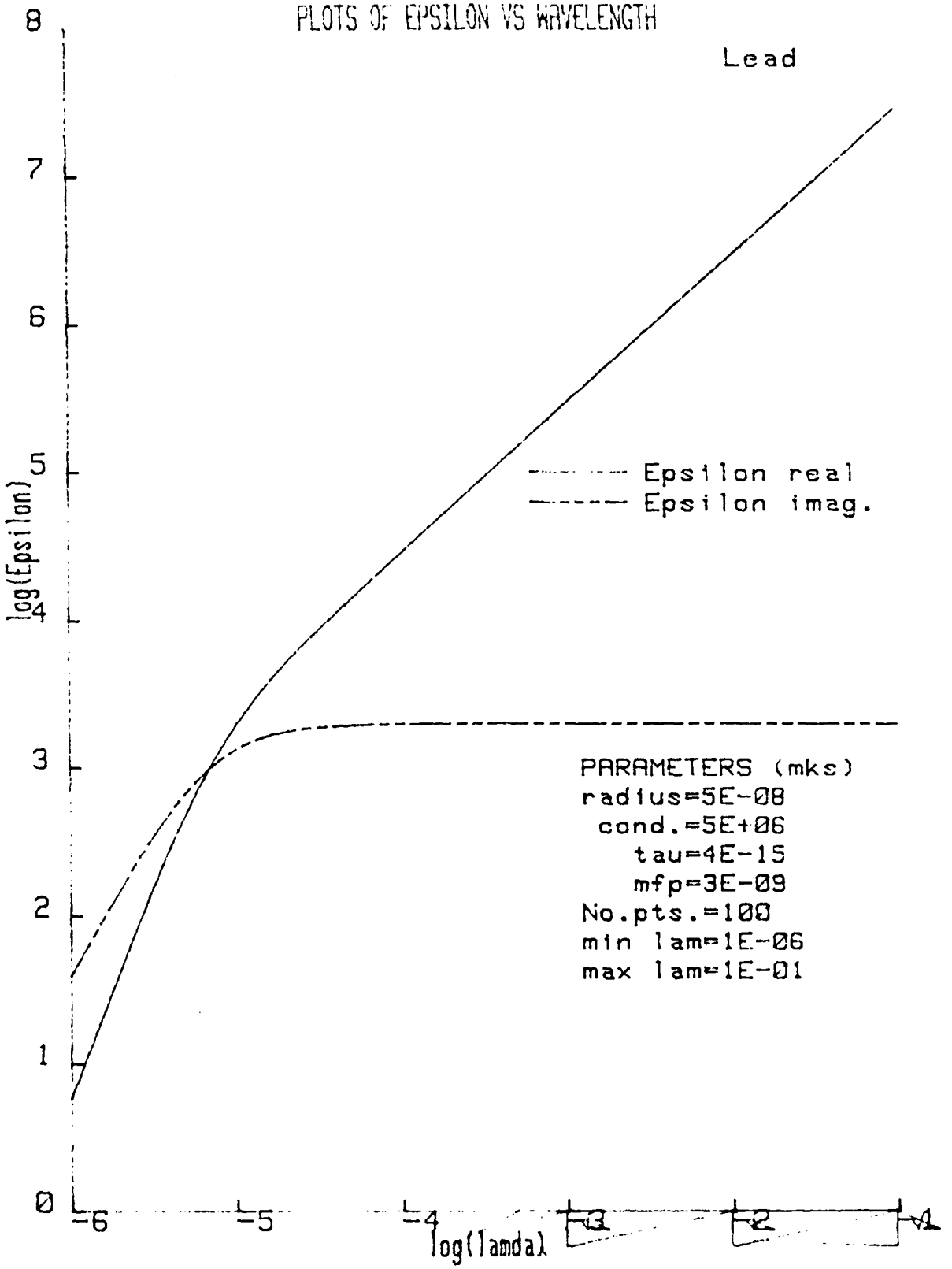

Fig. 13. Complex dielectric constant vs. wavelength for lead.

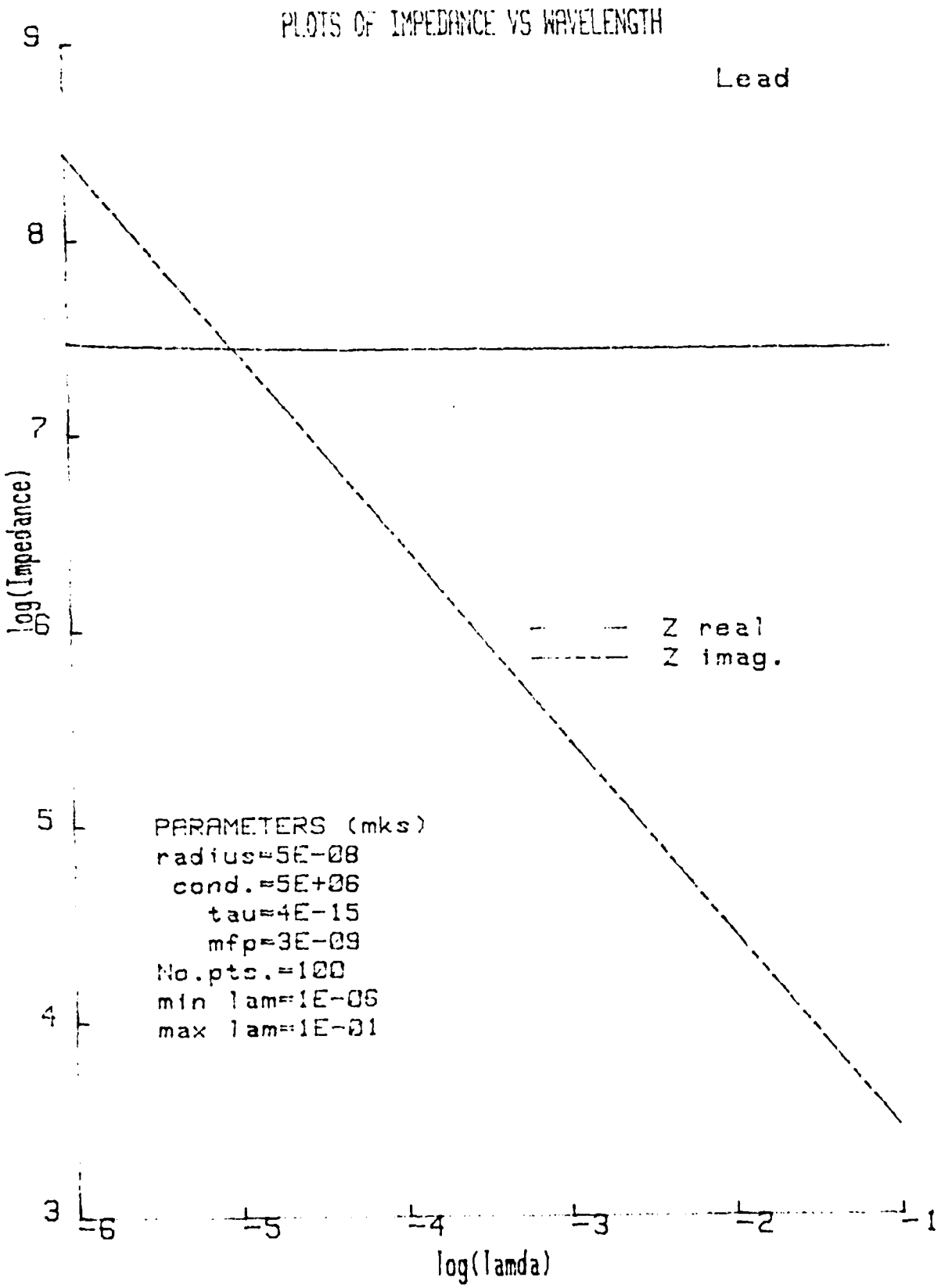

Fig. 14. Complex surface impedance vs. wavelength for lead.

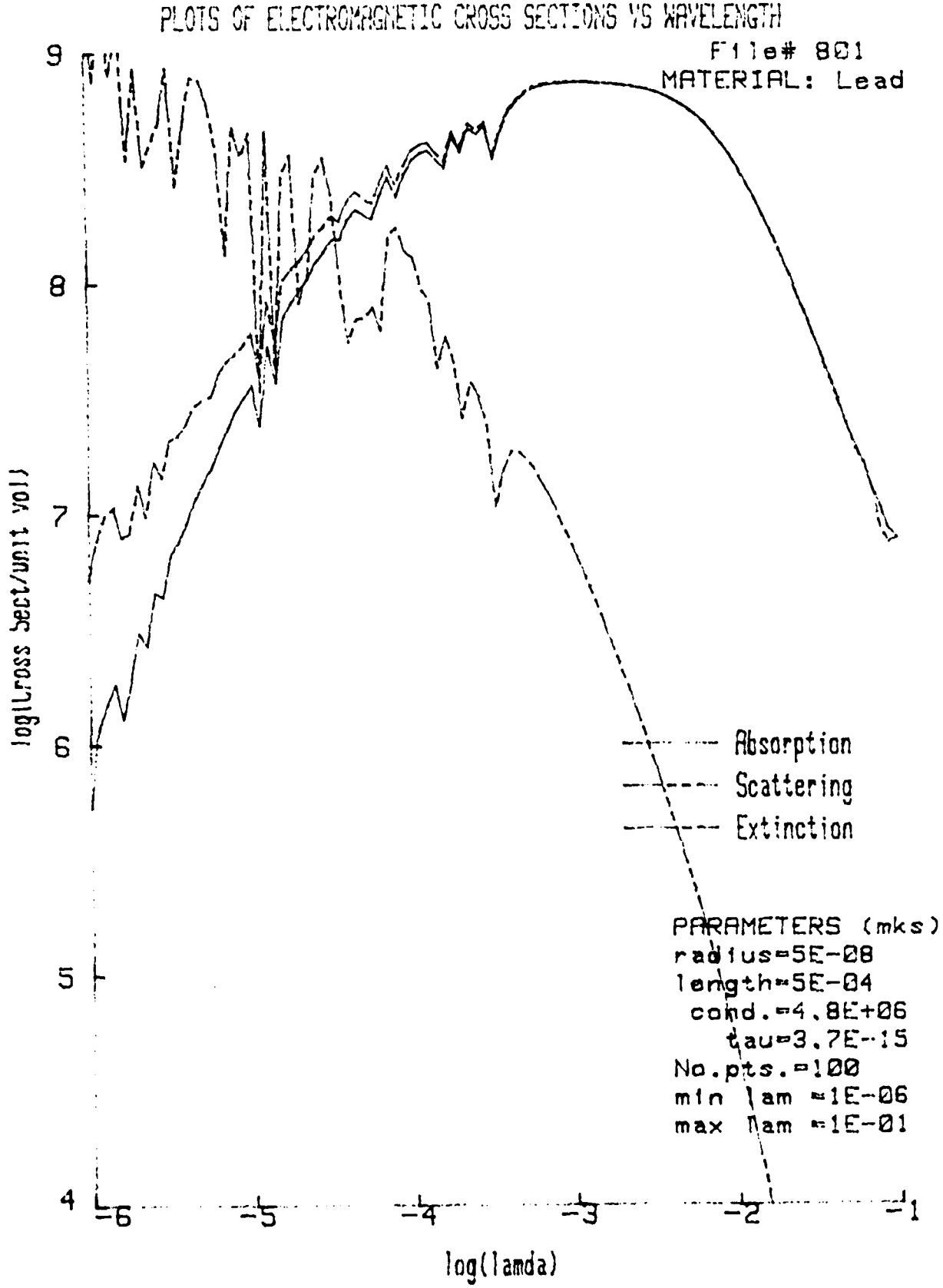

Fig. 15. Cross-sections vs. wavelength for lead (variational method).

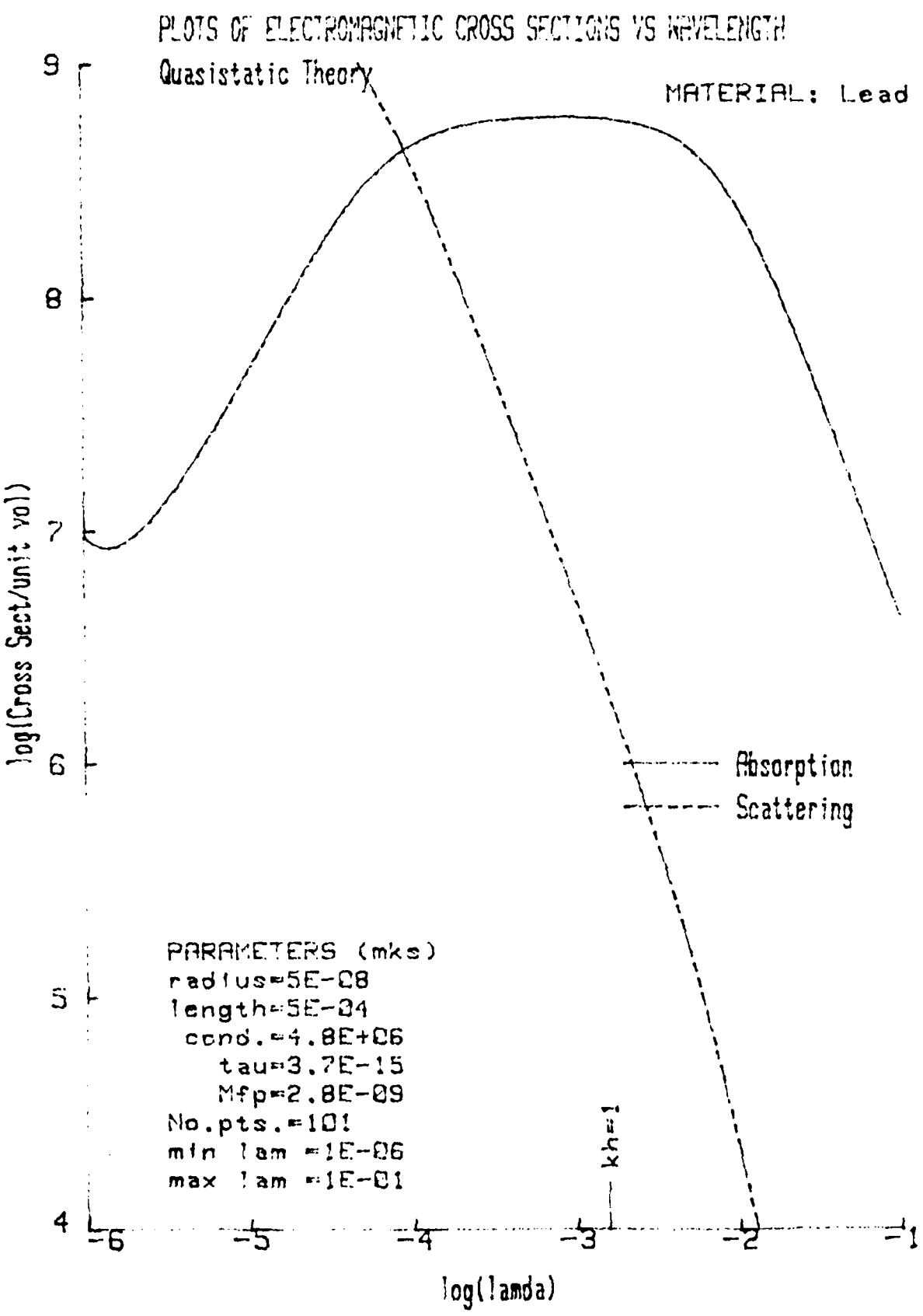

Fig. 16. Cross-sections vs. wavelength for lead (quasistatic theory).

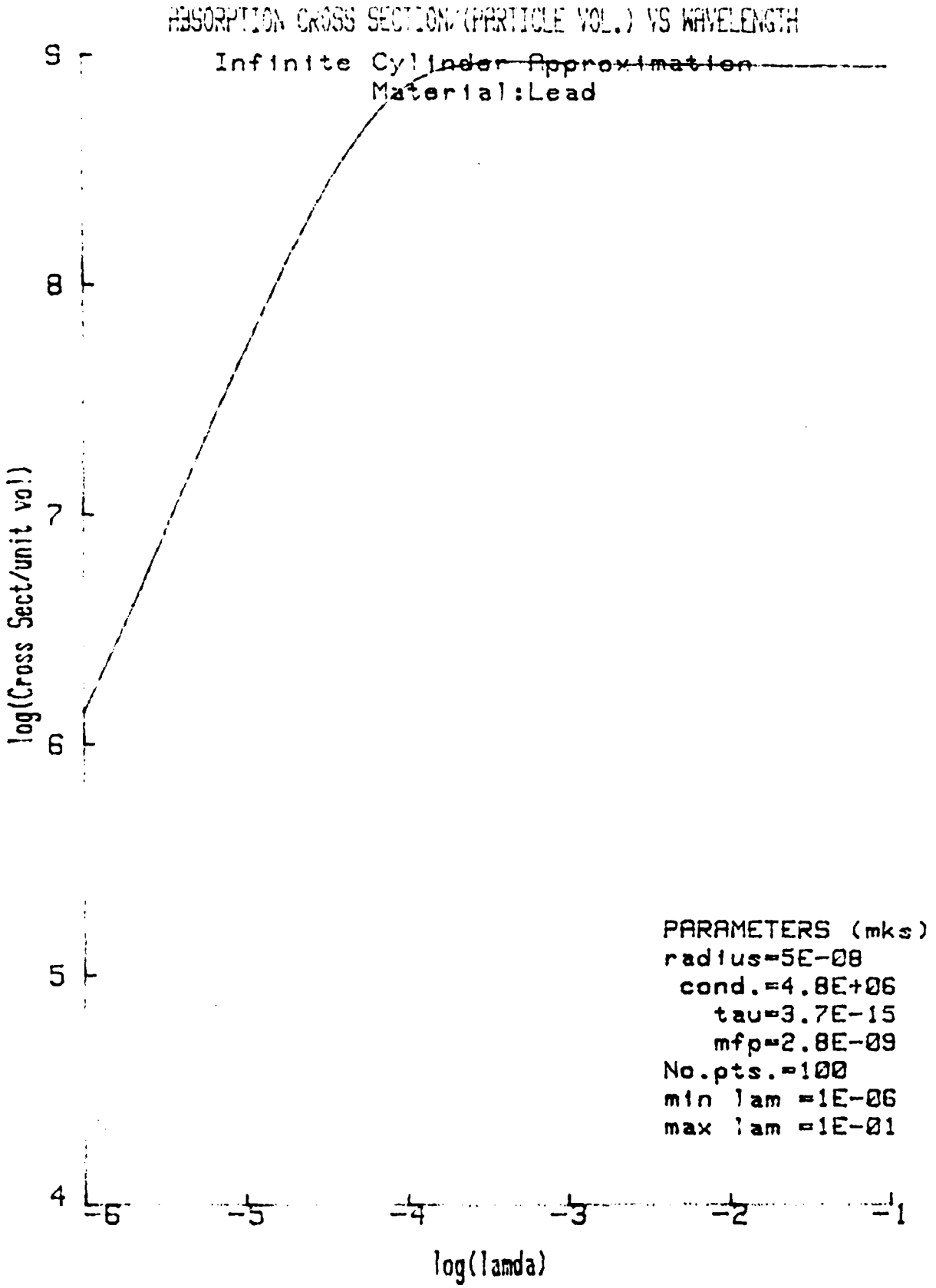

Fig. 17. Absorption cross-section vs. wavelength for lead (infinite cylinder approximation).

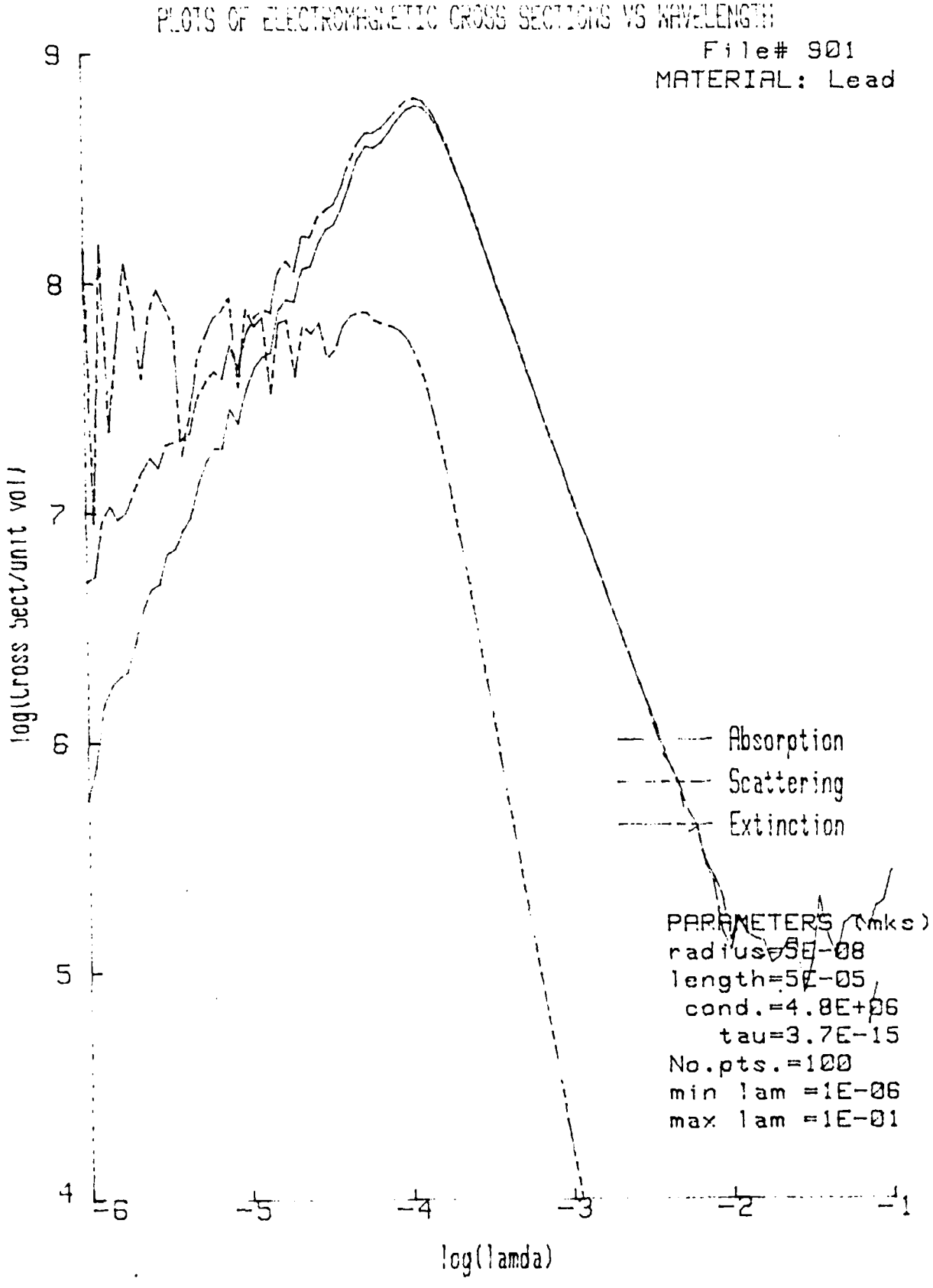

Fig. 18. Cross-sections vs. wavelength for lead (variational method).

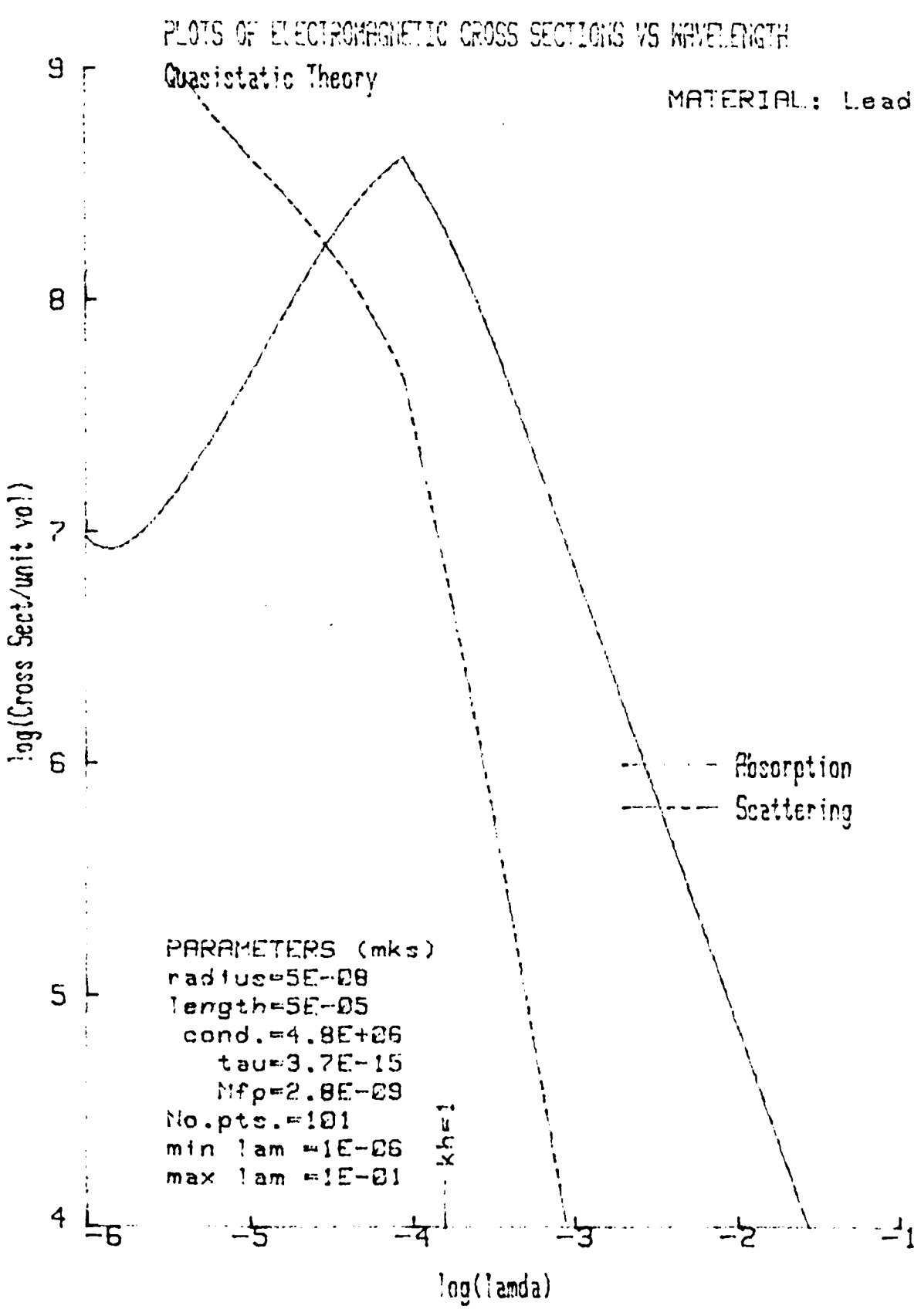

Fig. 19. Cross-sections vs wavelength for lead (quasistatic theory).

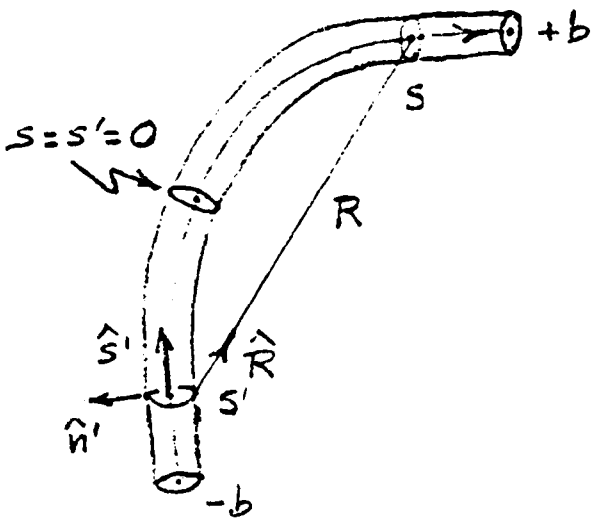

Fig. 20. Geometry of the Curved Fiber.

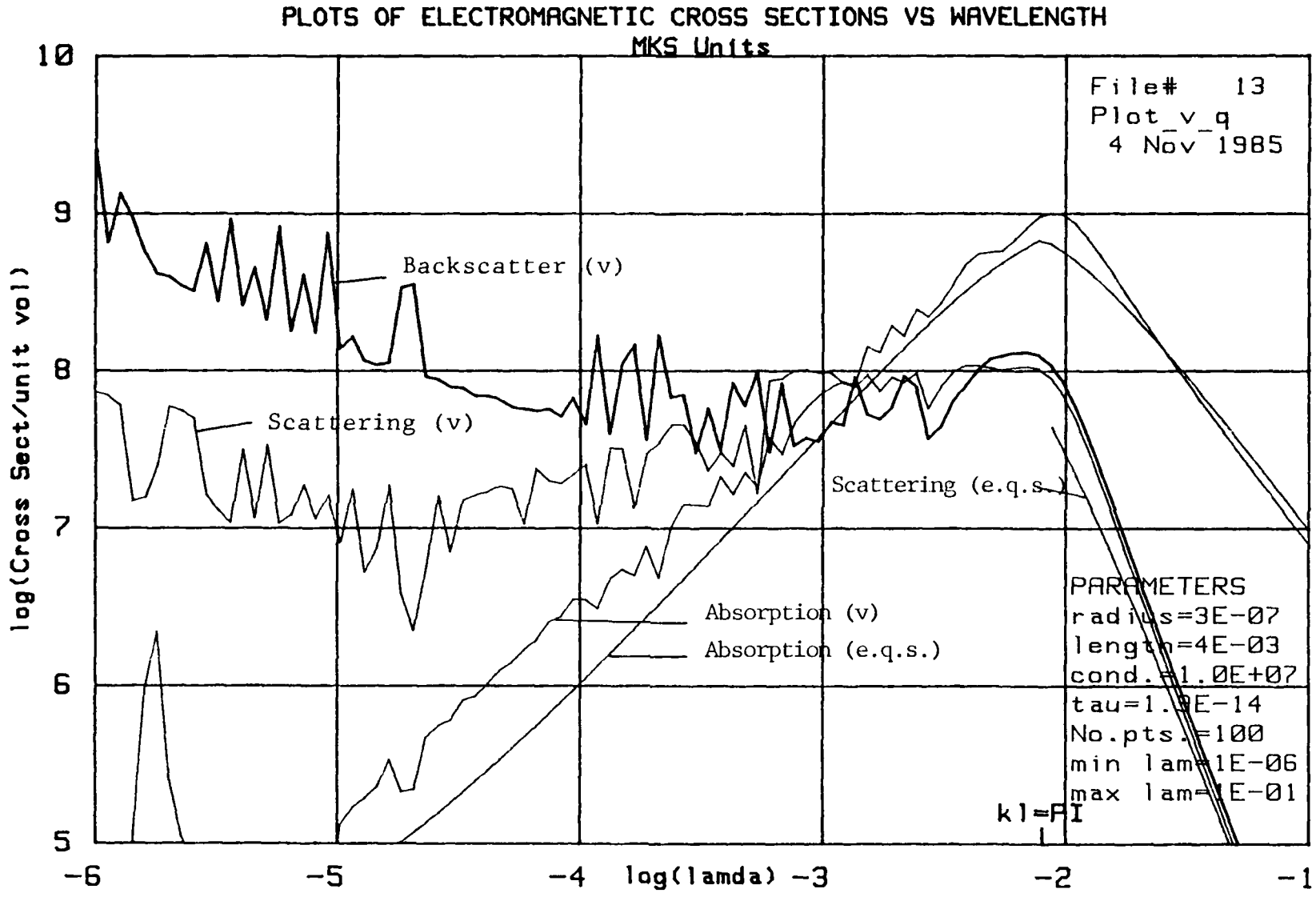

Fig. 21. An example of predominant at λ = 3 cm and predominant scattering at 300 microns. v = Variational technique; e.q.s. = Extended Quasistatic Theory.

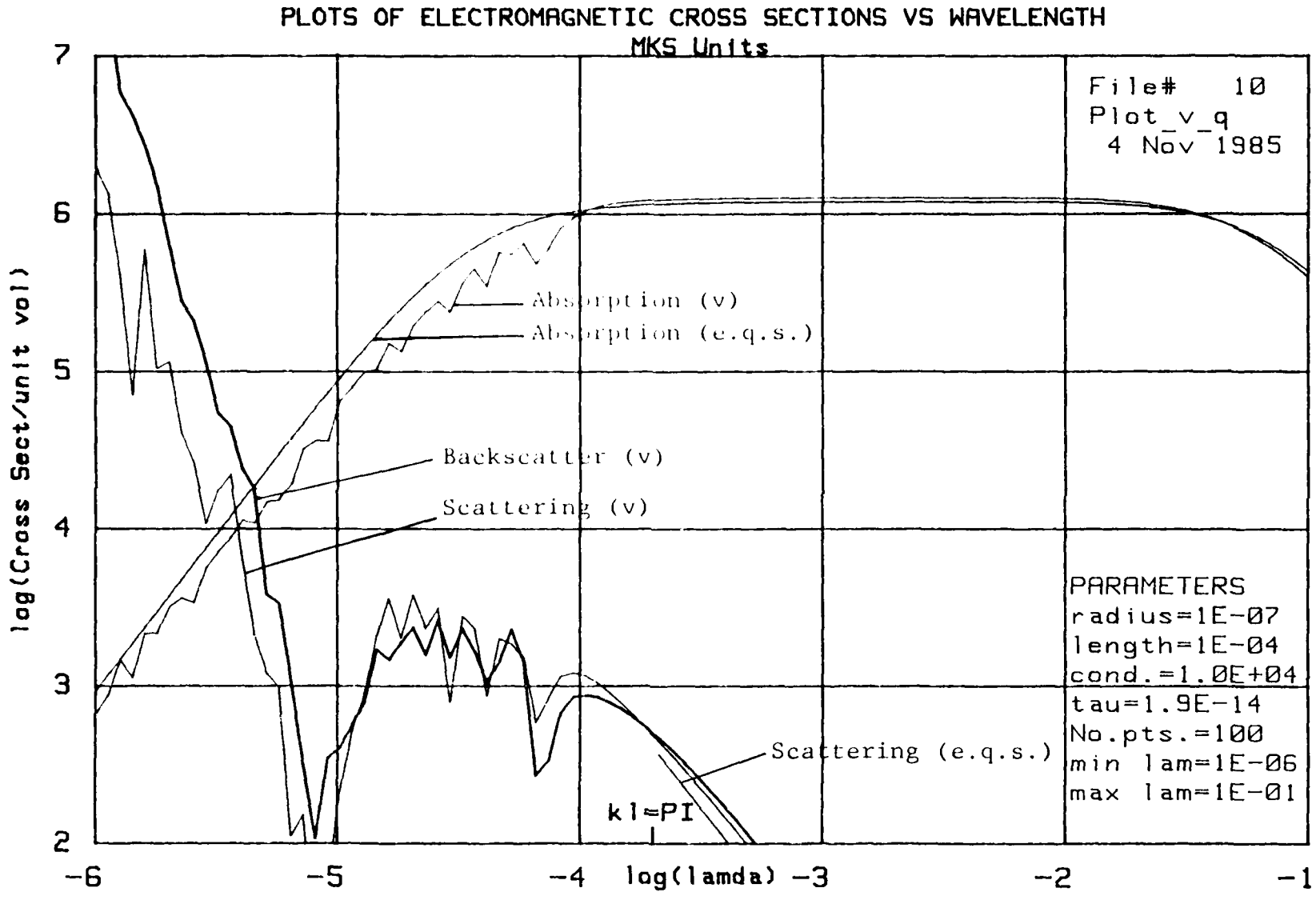

Fig. 22. An example of broadband absorption at 3 cm and 300 microns. v = Varitional technique; e.q.s. = Extended Quasistatic Theory.

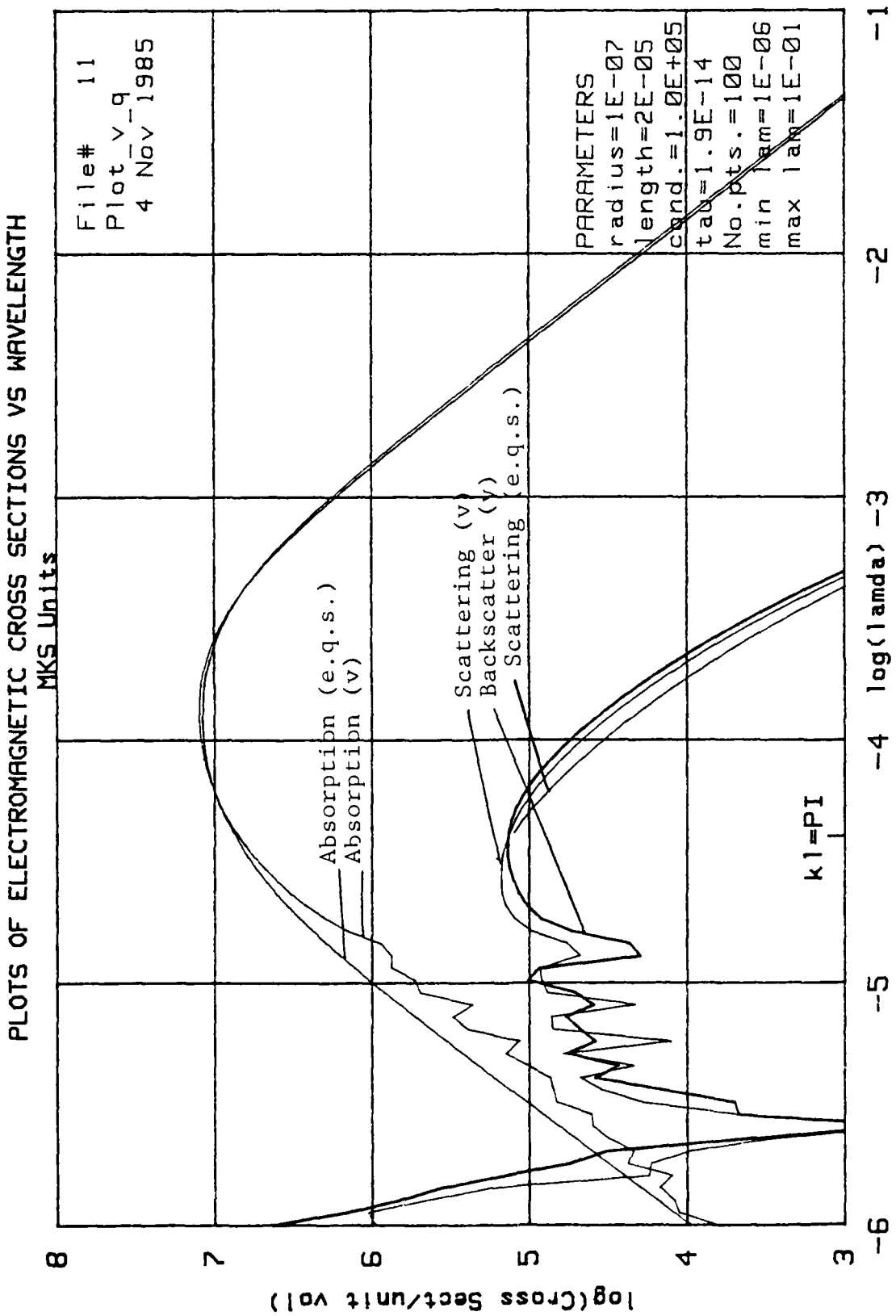

Fig. 23. An example of transparency at 3 cm and predominant absorption at 300 microns.

END

DTIC

9-86